

1 Highlights

2 **Accurate Determination of the Electron Spin Polarization In Mag-**
3 **netized Iron and Nickel Foils for Møller Polarimetry**

4 D. C. Jones, J. Napolitano, P. A. Souder, D. E. King, W. Henry, D. Gaskell,
5 K. Paschke

- 6 • Magnetization of Fe and Ni at room temperature from world data
7 • Spin fraction of magnetic moment for Fe and Ni from world data

8 Accurate Determination of the Electron Spin
9 Polarization In Magnetized Iron and Nickel Foils for
10 Møller Polarimetry

11 D. C. Jones^{a,*}, J. Napolitano^a, P. A. Souder^b, D. E. King^{a,c}, W. Henry^c, D.
12 Gaskell^c, K. Paschke^d

13 ^a*Temple University, Philadelphia, PA, 19122*

14 ^b*Syracuse University, Syracuse, NY 13244*

15 ^c*Jefferson Lab, Newport News, VA 23606*

16 ^d*University of Virginia, Charlottesville, VA 22903*

17 **Abstract**

18 The Møller polarimeter in Hall A at Jefferson Lab in Newport News, VA,
19 has provided reliable measurements of electron beam polarization for the
20 past two decades. Past experiments have typically required polarimetry at
21 the 1% level of absolute uncertainty which the Møller polarimeter has de-
22 livered. However, the upcoming proposed experimental program including
23 MOLLER and SoLID have stringent requirements on beam polarimetry pre-
24 cision at the level of 0.4%[1, 2], requiring a systematic re-examination of all
25 the contributing uncertainties.

26 Møller polarimetry uses the double polarized scattering asymmetry of a
27 polarized electron beam on a target with polarized atomic electrons. The
28 target is a ferromagnetic material magnetized to align the spins in a given
29 direction. In Hall A, the target is a pure iron foil aligned perpendicular to
30 the beam and magnetized out of plane parallel or antiparallel to the beam
31 direction. The acceptance of the detector is engineered to collect scattered
32 electrons close to 90° in the center of mass frame where the analyzing power
33 is a maximum (-7/9).

One of the leading systematic errors comes from determination of the target foil polarization. Polarization of a magnetically saturated target foil requires knowledge of both the saturation magnetization and g' , the electron g -factor which includes components from both spin and orbital angular momentum from which the spin fraction of magnetization is determined. Target foil polarization has been previously addressed in a 1997 publication “A pre-

^{*}Preprint submitted to Nuclear Inst. and Methods in Physics Research, A, September 26, 2022
Email address: donald.d.jones@temple.edu, jonesdc@jlab.org (D. C. Jones)

cise target for Møller polarimetry” by deBever *et. al* [3] at a level of precision sufficient for experiments up to this point. Several shortcomings with the previous published value require revisiting the result prior to MOLLER. This paper utilizes the existing world data to provide a best estimate for target polarization for both nickel and iron foils including uncertainties in magnetization, high-field and temperature dependence, and fractional contribution to magnetization from orbital effects. We determine the foil electron spin polarization at 294 K to be 0.08020 ± 0.00018 (@4 T applied field) for iron and 0.018845 ± 0.000053 (@2 T applied field) for nickel. We conclude with a brief discussion of additional systematic uncertainties to Møller polarimetry using this technique.

34 *Keywords:*

35 1. Introduction to Møller polarimetry

36 Møller polarimetry utilizes the analyzing power of polarized electron-
 37 electron scattering to determine the polarization of an electron beam. The
 38 polarized target is usually composed of iron or a highly ferromagnetic ma-
 39 terial. Elastically scattered events (beam electrons from atomic electrons)
 40 produce back-to-back electrons in the center of mass frame. If both are de-
 41 tected in coincidence background contributions can be significantly reduced.

Following the analysis in [4], where the center of mass energy of the e^-e^- pair $E_{CM} \gg m_e$, Møller scattering at tree level in the electron-electron center of mass (CM) system is given by

$$\frac{d\sigma}{d\Omega_{cm}} = \frac{\alpha^2}{E_{CM}^2} \frac{(3 + \cos^2 \theta)^2}{\sin^4 \theta} \left[1 - P_\ell^{\text{targ}} P_\ell^{\text{beam}} A_\ell(\theta) - P_t^{\text{targ}} P_t^{\text{beam}} A_t(\theta) \cos(2\phi - \phi_{\text{beam}} - \phi_{\text{targ}}) \right] \quad (1)$$

42 where the subscripts t and ℓ refer to transverse and longitudinal polarization
 43 respectively. The CM scattering angle is θ and ϕ is the azimuthal angle of
 44 the scattering plane. $\phi_{\text{beam(targ)}}$ is the azimuthal angle of the transverse
 45 beam(target) polarization. The analyzing powers for longitudinal and trans-
 46 verse polarization are given by

$$A_\ell(\theta) = \frac{(7 + \cos^2 \theta) \sin^2 \theta}{(3 + \cos^2 \theta)^2} \quad \text{and} \quad A_t(\theta) = \frac{\sin^4 \theta}{(3 + \cos^2 \theta)^2}. \quad (2)$$

At $\theta = 90^\circ$, A_ℓ is at its maximum value of $7/9$ which is a factor of 7 larger than A_t giving Møller polarimetry much more sensitivity to longitudinal polarization. The optics of the Møller polarimeter in Hall A are tuned to accept events near this maximum analyzing power for longitudinal polarization. The Møller polarimeter in Hall A with its Fe foil polarized “out of plane” in the beam direction ($P_t^{\text{targ}} = 0$) is designed to measure the longitudinal polarization and be insensitive to the transverse polarization. Nevertheless, if the foil or magnetizing coils are not properly aligned and a transverse foil polarization develops, a non-negligible component of transverse asymmetry could in principle arise. In the ensuing discussion it will be assumed that the foil is properly aligned such that $P_t^{\text{targ}} = 0$ and this term will be neglected.¹

Integrating the cross section over the acceptance of the detector gives

$$\sigma \propto 1 - P_\ell^{\text{targ}} P_\ell^{\text{beam}} A_{zz},$$

where $A_{zz} = \langle A_t(\theta) \rangle$, the acceptance-weighted analyzing power. We can now see that the left-right scattering asymmetry A_{LR} is then given by

$$A_{LR} = \frac{\sigma_R - \sigma_L}{\sigma_R + \sigma_L} = P_\ell^{\text{targ}} P_\ell^{\text{beam}} A_{zz}, \quad (3)$$

where $\sigma_{L(R)}$ are the cross sections for left (right) helicity electrons. Implicit in this form is the assumption that P_ℓ^{beam} is the same for both helicity states. If A_{zz} and the target polarization P_ℓ^{targ} are known, the beam polarization can be determined from the measured scattering asymmetry.

In the approximation where the target electrons are at rest and the beam energy is large compared to the electron rest mass m_e , the relationship between the lab momentum of the scattered electron, p' , and the center of mass scattering angle θ is given by

$$p' = \frac{p_b}{2} (1 + \cos \theta), \quad (4)$$

¹We can approximate the relative size of this term to justify our neglect of it. Longitudinal polarization at JLab can be adjusted for experiments to within $\pm 2^\circ$ of uncertainty, leaving a maximum P_t^{targ} of 0.035. Assuming an anomalously large transverse component of the target polarization due to misalignment of 5% and a transverse analyzing power that is approximately 1/7 that of the longitudinal gives a maximum transverse polarization contribution (i.e. for a beam and target polarization at the same azimuthal angle) that is 0.025% that of the longitudinal term.

where p_b is the electron beam momentum. Thus momentum analyzing the Møller scattered electrons also analyzes in θ . Single arm Møller polarimeters leverage this characteristic to reduce potentially overwhelming backgrounds arising from Mott scattering from the nucleus. Using a narrow aperture in ϕ to select the scattering plane and a dipole to momentum analyze the scattering events perpendicular to the scattering plane produces a characteristic Møller “stripe” downstream of the dipole. Converting to the lab scattering angle and in the absence of other focussing optics, and using the small angle approximation yield the following relationship between θ_{Lab} and momentum:

$$\theta_{\text{Lab}}^2 = 2m_e c \left(\frac{p_b - p'}{p' p_b} \right). \quad (5)$$

1.1. The Møller polarimeter in Hall A at Jefferson Lab

Part of the standard equipment in Hall A at Jefferson Lab is the Møller polarimeter, used to measure the electron beam polarization in the Hall. Most experiments in the past have had polarization requirements at the several percent uncertainty level easily attained by the Møller. Two recent experiments, PREX-2[5] and CREX, have reached $<0.9\%$ uncertainty for Møller polarimetry. However, MOLLER and SoLID, the future parity violation experiments planned for Hall A in 2025 and beyond, require uncertainty in electron polarization at $\pm 0.4\%$, a record-breaking level of precision that requires re-examination of all the possible sources of systematic error. This paper is designed to address specifically the uncertainty associated with target foil polarization for these experiments, but has obvious value for other Møller polarimeters around the world. Where appropriate, we will provide the means to extrapolate these results to other polarimeters with different designs and operating parameters.

The polarimeter in Hall A is designed to take advantage of both the dipole momentum selection and the coincidence of dual arm detection to further reduce backgrounds. A simple schematic of the Hall A polarimeter is shown in Fig. 1 illustrating the key features. This polarimeter design adds to the essential elements 4 quadrupoles and an additional horizontal constraint due to the narrow apertures through the dipole. The quadrupoles are used to focus a distribution of Møller pairs roughly symmetric about the 90 degree center of mass through the dipole onto the detector. The additional focusing of the quadrupoles inverts the expected typical quadrature curvature (see Eq. 5) of the Møller stripe on the detector plane as illustrated in Fig. 1.

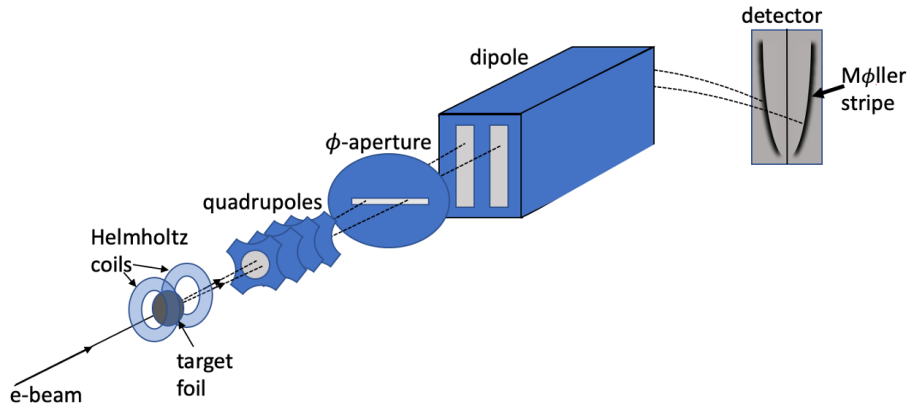


Figure 1: Simplified schematic showing the key features of the Møller polarimeter setup in Hall A. The electron beam scatters from a polarized foil target. Quadrupole magnets then focus the events of interest through the dipole magnet. An aperture at the front of the dipole limits the ϕ -acceptance, defining a horizontal scattering plane. Two left-right symmetric narrow vertical apertures in the dipole set the θ acceptance. The dipole momentum analyzes the scattered electron pairs bending them down onto the detector plane producing characteristic Møller stripes.

103 2. Foil Target Polarization

104 In the context of Møller polarimetry, the target polarization is produced
 105 using a strong magnetic field to align electron spins in ferromagnetic materials.
 106 The Møller polarimeter target in Hall A consists of a set of thin foils
 107 mounted on a target ladder and magnetized out of plane parallel (or anti-
 108 parallel) to the beam trajectory by a set of superconducting Helmholtz coils.
 109 The superconducting magnet used to polarize the target foils was built by
 110 American Magnetics Inc. The field at the center of the coils is horizontal and
 111 along the beam-line axis. The maximum field at the center is rated at 5 T,
 112 although we do not typically run above 4 T.

113 The three ferromagnetic elements, Fe, Co and Ni are the obvious choices
 114 for foil targets due to their relatively high magnetization and the precision
 115 with which their magnetic properties are known. A list of the main properties
 116 of these elements is given in Table 1. The saturation magnetization of Fe and
 117 Ni are both known to high accuracy ($\sim 0.2\%$), but the low Curie temperature
 118 of Ni makes it susceptible to large (percent level) corrections from target
 119 heating effects. There are fewer published measurements of high precision
 120 on Co than on the other two ferromagnetic elements.

Table 1: Properties of the three ferromagnetic elements. This manuscript focusses on the absolute uncertainties on M_0 and g' .

	Fe	Co	Ni
Z	26	27	28
Atomic Mass (μ)	55.845(2)	58.933194(4)	58.6934(4)
Electron Configuration	[Ar]4s ² 3d ⁶	[Ar]4s ² 3d ⁷	[Ar]4s ² 3d ⁸
Unpaired Electrons	2.2	1.72	0.6
Density near r.t. (g/cm ³)	7.874	8.900	8.902
M_0 at 0 K (emu/g)	222	164	58.6
g'	1.92	1.85	1.84
Curie Temperature (K)	1043	1400	631
Stable Isotopes	⁵⁴ Fe (5.85%) ⁵⁶ Fe (91.75%) ⁵⁷ Fe (2.12%) ⁵⁸ Fe (0.28%)	⁵⁹ Co (100%)	⁵⁸ Ni (68.08%) ⁶⁰ Ni (26.22%) ⁶¹ Ni (1.14%) ⁶² Ni (3.64%) ⁶⁴ Ni (0.93%)

121 Møller polarimetry requires finding the average target electron polariza-
122 tion which is most accurately known at magnetic saturation when further
123 polarization is negligible with increases in applied field. Determining the
124 target polarization requires knowing the magnetization of the target mate-
125 rial. Magnetization, \mathbf{M} , is defined as the magnetic dipole moment per unit
126 volume or in certain contexts, per unit mass. The magnetization provides
127 the magnetic field contributed by a material and relates the flux density \mathbf{B}
128 to the auxiliary field \mathbf{H} as follows:

$$\mathbf{B} = \mathbf{H} + 4\pi\mathbf{M}.$$

129 Note that this is in Gaussian units which are used throughout this document.

130 While knowledge of magnetization is key to determining target polar-
131 ization, it includes contributions of both the orbital and spin magnetic mo-
132 ments. Since we only want the spin component we need to find the fraction of
133 the magnetization that comes from spin. This is typically determined from
134 precise measurements of the gyromagnetic ratio (the ratio of a material's
135 magnetization to its angular momentum) of an elemental sample. Thus, the
136 final error on the target polarization will include uncertainties on both the

137 determination of magnetization and of the spin fraction.

138 In the following sections we look at each of the three elements and de-
139 termine the systematic uncertainty associated with using each as a target
140 materials. The primary issues to be dealt with are follows:

- 141 • From 1930-1980 many precise measurements have been made of the
142 magnetization and gyromechanical properties of these elements; how-
143 ever, they do not necessarily agree within error. Sometimes the errors
144 quoted are not realistic given the systematic disagreement in the data.
145 The sources of systematic difference are often not known and yet results
146 are averaged together and the final error estimated from the variance
147 of the data.
- 148 • No mention is made of the nuclear contribution to the magnetic mo-
149 ment. The nuclear magneton is smaller than the Bohr magneton by a
150 factor of $m_e/m_p \sim 0.05\%$. Fortunately, the main isotopes that make up
151 iron and nickel are even-even and have spinless nuclei, but for Co the
152 average is 4.6 nuclear magnetons making the contribution potentially
153 above the 0.1%.
- 154 • Measurements of magnetization and gyromechanical properties are not
155 made at the same applied field and temperature where the Møller po-
156 larimeter operates, necessitating corrections to account for these differ-
157 ences. The corrections must be known to sufficient accuracy and the
158 conditions under which the measurements were taken must be known.
- 159 • Through the past century measurement of constants have become more
160 precise and have changed. Examples of constants used in determining
161 quoted magnetization and gyromagnetic data in the literature are the
162 density of elements, the charge to mass ratio of the electron, and the
163 Bohr magneton. Different groups use different values. Sometimes the
164 values of constants used in calculations (eg. the Bohr magneton) are
165 assumed to be known and are not given.
- 166 • Experiments measuring properties of these ferromagnetic elements used
167 different levels of purity. It is not clear what uncertainty should be
168 assigned to account for the effects of impurities.
- 169 • In many publications, the data are only shown as plots and the values
170 of the measurements are not provided. The values must be extracted

with plot digitization software.

- In order to compare magnetization data taken with different sample shapes, the applied field must be converted to the internal field, H_{int} . This conversion is not always possible if the data are not given in terms of H_{int} or the sample shape and dimensions are not provided so that this conversion from applied to internal field can be made.

2.1. Determining Saturation Magnetization

Target polarization is determined from measurements of the saturation magnetization. Another term used in the literature is “spontaneous magnetization,” which, as the name implies, refers to the magnetic moment of a material that spontaneously arises with no applied field. In ferromagnetic materials the magnetic moments of the electrons tend to spontaneously align in a given direction. However, due to energy considerations, domains tend to form in such a way that the total spin averaged across many domains at the macroscopic level is far below the saturation level and may be zero. In the presence of an applied magnetic field, the domain boundaries shift with enlarging domains having magnetic moments aligned along the direction of the field. As the applied field is increased, eventually the material will reach magnetic saturation where all the spins are aligned along the direction of the applied field. Thus, the saturation magnetization and the spontaneous magnetization are related quantities and spontaneous magnetization is numerically equal to the saturation magnetization at 0 K. Quoting from [6]: “Under a sufficiently high external magnetic field, the sample reaches saturation and represents a single-domain system oriented along this field direction. Therefore, the saturation magnetization can be considered to be equal (to) the spontaneous magnetization of one domain.” For a discussion of domain formation and saturation magnetization see Kittel’s Review paper from 1949[7].

2.1.1. Temperature and Field Dependence of Saturation Magnetization

Spontaneous magnetization is a function of temperature and applied field and for this reason it is often given as M_0 , the value of saturation magnetization extrapolated to zero applied field at $T = 0$ K. However, experiments measure the magnetization at temperatures above 0 K with non-zero applied fields. For temperatures well below the Curie temperature and low applied

fields, the magnetization has been shown to roughly follow the $T^{3/2}$ law of Bloch given as [8]

$$M_s(T) = M_0(1 - a_{3/2}T^{3/2}), \quad (6)$$

where M_0 is the saturation magnetization at 0 K and $a_{3/2}$ is an empirically determined constant.

This temperature-dependence of the saturation magnetization arises primarily from the presence of spin-waves which are traveling excitations of spin precessions about the magnetic field propagating through a material. Spin waves propagate via coupling between neighboring spins and are strongly temperature-dependent with thermal energy driving the excitations. Near absolute zero, spin waves are nearly absent and their increased effect with temperature causes saturation magnetization to decrease with temperature as the overall alignment of individual atomic moments with the applied field decreases. Increasing the applied field also decreases the effect of spin waves so that at high fields and low temperature their effect is diminished. For a more detailed discussion of spin waves see [9, 10, 11, 12].

At higher fields and temperatures not small compared to the Curie temperature additional terms are required beyond those included in Eq. 6. Freeman Dyson used an expansion in powers of T to parameterize the dependence of saturation magnetization on temperature and applied field[13, 10]. Frederic Keffer building on the work of Dyson and others developed a more elaborate form of the expansion with terms depending on $T^{3/2}$, $T^{5/2}$, $T^{7/2}$ and T^2 as well as the strength of the internal field[14]. The half-power terms in T arise from spin waves and the T^2 term accounts for the possibility of Stoner-type excitations from the band structure in metals[15].

This parameterization, while accounting for temperature and field dependence arising from spin waves, fails to account for the nearly linear high-field paramagnetic susceptibility of ferromagnets well above saturation as well as effects unique to each sample which prevent saturation and thought to arise from impurities, strains, anisotropy, domains and even the geometry of the sample[11]. Foner *et al.* divide magnetization data into three regions: 1. the low-field region approaching saturation where the aforementioned sample-dependent effects prevent saturation at the theoretical saturation value and create curvature unique to each sample in the M versus H_{int} curves just below saturation; 2. the high-field region above saturation where effects from spin waves and possible remnant anisotropy remain in addition to the high-field susceptibility; 3. and the ultra-high field region where magnetic phase

transitions may exist and which is not of interest here[11]. These considerations suggest that use of Keffer's parameterization may require additional terms to account for the linear high-field susceptibility as well as non-linear curvature in the approach to saturation.

Pauthenet performed an extremely precise measurement of the saturation magnetization of Fe and Ni as a function of both temperature and internal field from 0 to 17 T. Pauthenet claims the absolute scale in his measurements is known only to $\pm 0.5\%$ due to uncertainty in calibration but that relative uncertainty is at the 0.01% level, making his work an authoritative reference for high field corrections. Following the work of Keffer, he expressed the saturation magnetization M as a function of temperature and internal field, while adding a term linear in applied field, $\chi(T)$, to account for the known effect of high field susceptibility:[14, 12, 15]

$$M(H_{\text{int}}, T) = M_0 \left(1 - \sum_{s=\frac{3}{2}, \frac{5}{2}, \frac{7}{2}} a_s \frac{F(s, t_H)}{\xi(s)} T^s - a_2 T^2 \right) + \chi(T) H_{\text{int}}. \quad (7)$$

Here M_0 is the spontaneous magnetization at 0 K and zero applied field, $F(s, t_H) = \sum_{p=1}^{\infty} p^{-s} e^{-pt_H}$ is the Bose-Einstein integral function, and $t_H = g\mu_B H_{\text{int}}/k_B T$, where g is the Landé g-factor, μ_B is the Bohr magneton, and k_B is the Boltzmann constant. H_{int} is the internal field and $\xi(s)$ is the Riemann zeta function. Pauthenet fits this parameterization to his data to give numerical values for the coefficients, providing magnetization as a function of internal magnetic field and temperature (see Eq. 9, 10 and Table 1 from [12]). We use Pauthenet's numerical parameterization of magnetization as a function of internal field and temperature provided in Eqs. 9 and 10 of [12], to make corrections for differences in temperature and internal field.

It is important to note the difference between internal field and applied field. In a manner somewhat analogous to the internal electric field cancellation inside a dielectric, the applied magnetic field is partially cancelled inside a ferromagnetic sample by its magnetization. The relationship between the internal field and the applied field is given by the following equation (in the cgs system)

$$H = H_{\text{int}} + \frac{4\pi M}{\rho}, \quad (8)$$

where H is the applied field, H_{int} is the internal field, M is the magnetization and ρ is a demagnetization constant that depends on the shape of the sample.

Since the internal field is thus partially cancelled by the magnetization, $4\pi M$ is sometimes referred to as the “demagnetizing field”.

Well below saturation, the internal field is nearly 0 due to the demagnetizing field. In the literature, field-dependent corrections are often given as a function of internal field H_{int} not applied field H . Above saturation magnetization, H_{int} is less than H by the saturation magnetization (21.58 kOe for iron and 6.2 kOe for nickel). There appear to be errors in the literature that stem from incorrect exchanges of applied field and internal field. For example, Eq. 3 from deBever *et al.* incorrectly interprets Pauthenet’s corrections as a function of flux density B instead of internal field. As a result, they calculate a correction from an applied field of 1 T to the final value of 4 T. A 4 T field applied normal to a thin Fe foil such as they were discussing translates into an internal field of ~ 1.8 T for Fe foils, requiring a smaller correction. C. D. Graham also appears to confuse the two in Fig. 5 of [16] where he plots magnetization versus $1/H$ but combines data from multiple sources some of which are in terms of $1/H$ and others which are in terms of $1/H_{\text{int}}$.

2.1.2. Other Factors Affecting Magnetization Measurements

There are several issues to be aware of when trying to interpret magnetization values quoted in the literature.

Shape anisotropy: the magnetization depends upon the shape of the object. Needles are very easy to magnetize along their long axis but much more difficult along a direction perpendicular to it. Each shape has a characteristic demagnetizing factor ρ (see Eq. 8) that is a function of the direction of applied field (unless symmetry dictates otherwise). Perfect spheres have a demagnetizing factor of $3/4$. The demagnetizing factor for ellipsoids of rotation is a function of the ratio of the two axis lengths. Figure 2 shows the demagnetizing factor of ellipsoids of rotation as a function of the axis ratio where the applied magnetic field is along the axis R_z . A thin foil disk such as that used in the Møller polarimeter can be taken to be a flattened ellipsoid with an axis ratio of ~ 0 . In this case the demagnetizing factor approaches unity[17].

Crystal anisotropy: the crystal structure of a material can create directions along which it is easier to magnetize. The direction along which magnetic saturation is reached with the smallest applied field is called the easy axis of the crystal. Monocrystalline nickel, for example, has three different magnetization axes termed the [111], [110] and [100] axes, using standard

310 Miller index notation, with [111] being the easy axis. Therefore, if one is us-
 311 ing monocrystalline materials, the magnitude of the external field required
 312 to reach saturation will depend upon alignment of the crystal relative to the
 313 field. For polycrystalline materials there will be no preferred direction as a
 314 result of the random crystal orientations.

315 **Crystal structure and phase changes:** some crystals have more than
 316 one possible crystal structure with different magnetizations. Their history
 317 of heating/cooling and annealing can have an effect on their magnetic prop-
 318 erties. Cobalt, for example, goes through a phase change when heated at
 319 690 K going from a close-packed hexagonal to a face-centered cubic crystal
 320 structure above 690 K which is unstable below that temperature. However,
 321 the exact crystal structure below 690 K (and by extension the magnetization)
 322 depends upon the grain size and the annealing process used to prepare it[18].

323 **Stesses and strains:** stresses and strains in the material as well as
 324 porosity will affect how easily the material is magnetized. This can be seen
 325 particularly well by annealing, which often makes the material more easily
 326 magnetized[19].

327 2.1.3. *Measurements of Saturation Magnetization*

328 Although different methods are used to measure the saturation magneti-
 329 zation, they broadly break down into two categories:

- 330 1. Force method: a small ellipsoid sample of the element of interest is
 331 placed in a precisely determined field gradient. With a proper setup,
 332 the force on the sample by the magnetic field can be shown to be
 333 the product of the magnetic moment of the sample and the magnetic
 334 field gradient. Thus the magnetic moment of the sample is given as
 335 the force divided by the field gradient. Dividing by the mass of the
 336 sample gives the mass magnetization directly. A possible source of
 337 systematic error in this method is the use of standard weights and
 338 a balance to measure forces. Conversion from mass to force requires
 339 knowing the gravitational acceleration at the measurement location and
 340 relative uncertainty in this value translates directly into the final result.
 341 Of the magnetization measurements included in this study, only those
 342 by Crangle *et al.* utilized this method.
- 343 2. Induction method: a sample is placed into a magnetic field and its
 344 presence creates a magnetic moment that is measured in pickup coils.
 345 This directly measures volume magnetization and must be converted

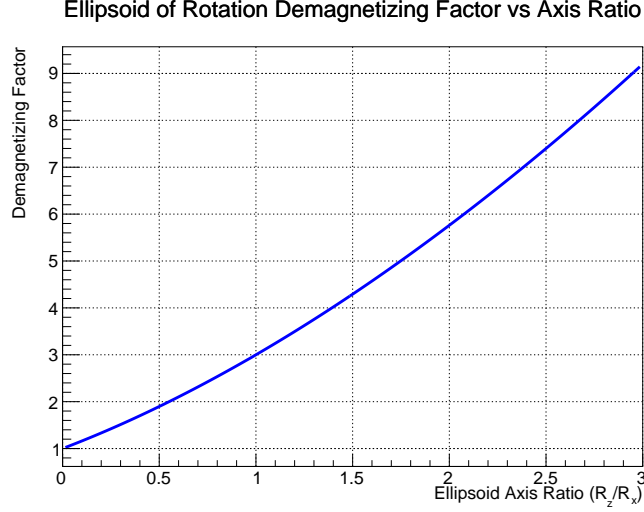


Figure 2: Demagnetizing factor for ellipsoids of rotation as a function of axis ratio for external magnetic field applied along the axis of rotation R_z . This plot uses equations 1a and 1b from [17].

346 to mass magnetization by multiplying by density, introducing another
 347 potential source of systematic error.

348 Although the experimental methods can be thus broadly categorized, each
 349 individual experiment takes a slightly different approach to measurement and
 350 calibration.

351 Measurements of magnetization are performed at a variety of applied
 352 magnetic fields and temperature and are typically expressed in terms of the
 353 saturation magnetization M_0 which is the extrapolation to zero applied field
 354 at 0 K[20]. A review of the literature yields many measurements of the
 355 magnetization of iron and nickel. Different approaches can be taken to ob-
 356 tain “consensus” values. One approach taken by H. Danan *et al.*[21] and
 357 deBever *et al.* [3] is to average the values of spontaneous magnetization
 358 $M_0(H = 0, T = 0 \text{ K})$ and then apply a correction to obtain the magnetiza-
 359 tion at room temperature and nonzero applied fields. However, the process of
 360 extrapolation to zero field and temperature is not standardized and different
 361 methods are utilized, making this a poor standard for comparison. Further-
 362 more, since we are looking for magnetization near room temperature this
 363 method introduces error extrapolating down to M_0 and once again correct-
 364 ing back up to room temperature and high fields. Since most measurements

at least include data at or near room temperature and at internal fields at or close to 10 kOe (1 T), it makes sense to utilize magnetization measurements taken near room temperature and internal fields of order 10 kOe. Where the available data in the literature were not available at precisely $T=294$ K, small corrections were applied to the measurements based upon the formulation given in [12]. In each case the data of magnetization versus internal magnetic field were parameterized using Eqs. 9 and 10 from [12].

Although the “consensus” values presented here for magnetization include data from a number of measurements done over a period from 1929-2001, this is not an exhaustive data set by any means. Table 2 lists the publications used in this analysis for iron and nickel. We established the following criteria to decide which data to include:

- Original data was published and publication was available. Some measurements referred to in the literature are not readily available. For example much of Danan’s reported measurements on Ni were never published except in his 1968 review which provides few details of the experiment.
- Data in the publication were available near room temperature (294 ± 10 K) and an internal field of 10 kOe. We corrected all data in this analysis to $T = 294$ K. Starting with measurements of the magnetization close to these values of temperature and internal field keeps the corrections and extrapolation uncertainty small.
- Enough details were provided to obtain the internal field of the sample either because the data were given versus internal field or the demagnetizing factor could be calculated from information given.
- Data were taken with a high purity sample. With the exception of the NASA study by Behrendt *et al.* for which purity was not stated, all samples used had greater purity than 99.9% to keep the systematic error from this source small. The NASA study was included in spite of the lack of information on sample purity because they claimed measurement error of $\pm 0.2\%$ and they were only the second data set we found with measurements in the high-field (several tesla) region of interest to us and which met the other criteria.
- Systematic errors were sufficiently small to provide useful additional information. For example, Pauthenet [12] has very precise data, but

400 since he uses Danan’s Ni data for absolute calibration, his systematic
 401 error is 0.5%. Therefore, Pauthenet’s data are used for relative correc-
 402 tions of field and temperature, but not in the absolute measurement
 403 average. Aldred [22] also has a precise data set, but calibrates his data
 404 using the “known magnetization of nickel” which is exactly what this
 405 analysis is seeking to determine. For this reason, we also did not retain
 406 Aldred’s data.

Table 2: Publications used in obtaining consensus value for magnetization near room temperature at high fields.

Publication	Year	T (K)	Comment
Weiss and Forrer [23]	1929	288	Only Fe data used
R. Sanford <i>et al.</i> (NIST)[24]	1941	298	Data on Fe only
H. Danan [25]	1959	288	Data on Ni and Fe
Arajs and Dunmyre [26]	1967	298	Data on Ni and Fe
Crangle and Goodman [20]	1971	293	Data on Ni and Fe
Behrendt and Hegland (NASA)[27]	1972	298.9	Data on Fe only
R. Shull <i>et al.</i> (NIST)	2000	298	Data on Ni only

407 Fig.3 shows the data for the magnetization of Fe from the published sources
 408 before and after correction to $T = 294$ K. Where data were not given in
 409 terms of internal field H_{int} , they were converted to H_{int} using Eq. 8 using
 410 information given in the publications to determine the demagnetizing field
 411 $4\pi M/\rho$. The data are approximately linear as expected in the high-field
 412 region above 3 kOe. The lower panel of Fig. 3 shows the data after correc-
 413 tion to the standard temperature 294 K. It is striking that the temperature
 414 correction increases the inconsistency between the different data sets. As pre-
 415 viously mentioned, the temperature correction was taken from Pauthenet’s
 416 parameterization given in Eq 9 in [12] (see Eq. 7) with the coefficients found
 417 empirically to be $a_{3/2} = 307 \times 10^{-6}$, $a_{5/2} = -22.8 \times 10^{-8}$ and $a_{7/2} = 0$. Pau-
 418 thenet evaluates the factor $g\mu_B/k_B$ as 1.378×10^{-4} .² A linear approximation
 419 $\chi(T) = 3.644 \times 10^{-6} + 5.0434 \times 10^{-10}T$ was obtained from a fit to the discrete

²Note that Pauthenet actually gives $g\mu_B/k_B = 1.378$ for Fe in Eq. 9 of [12], but replicating his plots in Figure 1 of [12] requires an extra factor of 10^{-4} .

420 data points provided in Table 1 of [12] in order to be able to evaluate $\chi(T)$
 421 for any temperature.

422 To get an average parameterization versus internal field, each of the six
 423 temperature-corrected data sets were fit individually using Pauthenet’s pa-
 424 rameterization with $T = 294\text{ K}$ as can be seen in Fig. 4. Pauthenet’s work
 425 was chosen as the high-field reference since he quotes the relative uncertainty
 426 of the data used in his fit to be at the 0.01% level and his parametrization in
 427 the high-field region accurately reproduces the field dependence seen in the
 428 data.

429 An additional term of a/H_{int}^2 was added to Pauthenet’s parameterization
 430 to provide a better fit at low internal field in the approach to saturation.
 431 Pauthenet’s data did not roll off as quickly as the data used here (see Fig.
 432 1 of [12]). The exact curvature in this region is expected to depend on the
 433 composition and purity in addition to stresses and imperfections in the sam-
 434 ple used which will vary from sample to sample. Pauthenet used a high
 435 purity monocrystalline sample aligned along the easy axis to suppress ef-
 436 fects from anisotropy and strains, whereas many of the datasets included
 437 here used polycrystalline samples, providing a plausible explanation of the
 438 discrepancies in this region.

439 Stoner discusses the interpretation of terms proportional to $1/H_{\text{int}}$ as
 440 arising from inclusions (impurities or cavities) in the sample and $1/H_{\text{int}}^2$ as
 441 arising from stresses and imperfections (see discussion around Eqs. 4.18-4.22
 442 in [28] and around Eq. 7 of [29]).

443 For the Fe datasets included here, the term proportional to $1/H_{\text{int}}$ was
 444 not needed, so only a term of the form a/H_{int}^2 was retained. The coefficient a
 445 was constrained to values 0 or below in the fit to maintain consistency with
 446 the physics model. For the data sets with measurements over a range of H_{int}
 447 both M_0 and a were used as fit parameters. In fits for two of the data sets
 448 (Weiss *et al.* and Sanford *et al.*), only M_0 was allowed to float due to the
 449 limited number of data points and a was fixed to the average from the data
 450 sets where it was allowed to float as a fit parameter. The data for Weiss and
 451 Forrer were not specifically given, but the following linear parameterization
 452 was provided from a fit to data over the range of applied fields from 0.6 to
 453 1.7 T: [23]

$$M_0(H) = 217.76 \left(1 - \frac{2.6}{H} \right),$$

454 where H is the applied field in oersteds. This parameterization was used to

determine two data points at 0.6 T and 1.7 T which were then fit to determine M_0 . The data for Sanford (NIST) *et al.* are condensed in the literature to a single value of H_{int} even though they are composed of multiple values across a range of applied fields not included in the publication.

The average value of M_0 and a from the fits were used to produce the average parameterization curve shown. Over the range of H_{int} from 8 to 28 kOe (about 3 to 5 T applied field for a thin Fe foil magnetized out of plane normal to the surface) the following second degree polynomial accurately follows the average parametrization curve:

$$M_{\text{sat}}^{(\text{Fe})}(H_{\text{int}}, 294 \text{ K}) = 217.628 + 2.7439 \times 10^{-2} H_{\text{int}} - 2.6304 \times 10^{-4} H_{\text{int}}^2, \quad (9)$$

where H_{int} is in units of kOe. This parameterization is shown in Fig.4. A systematic error band of $\pm 0.20\%$ is assigned to account for the spread of the data. The source of this systematic spread across the datasets is not clear.

Using 2.157 T for the magnetic saturation induction ($4\pi M_{\text{sat}}$) of iron and a demagnetizing factor of unity for a thin foil magnetized out of plane, gives an internal field which is 2.157 T less than the applied field near saturation. Thus a uniform external 4 T magnetic field corresponds to an internal field of approximately 1.84 T. Converting Eq. 9 to applied field B_{app} in Tesla (this is the field of the magnet alone without the induction of the foil) for the specific case of a thin foil magnetized out of plane gives the following second order polynomial parameterization accurate over the region of 3-5 T applied field:

$$M_{\text{sat}}^{(\text{Fe})}(\text{emu/g}) = 216.914 + 0.387863 B_{\text{app}} - 0.026304 B_{\text{app}}^2. \quad (10)$$

This gives the saturation magnetization per gram for iron at 294 K with an applied field of 4 T as $M_{\text{sat}}^{(\text{Fe})} = 218.04 \pm 0.44 \text{ emu/g}$. This translates into $2.1803 \pm 0.0044 \mu_B/\text{atom}$ which differs slightly from the value of $2.183 \pm 0.002 \mu_B/\text{atom}$ determined by deBever *et al.*[3] partially due to their over-correction for the magnetic field dependence. The small uncertainty quoted by deBever *et al.* comes from C. D. Graham's review [16] and uses the single data set of Crangle *et al.*[20] with a 0.1% uncertainty. Furthermore, this publication by deBever *et al.* also misinterprets the 1 T applied field for Crangle's elliptical sample as being equivalent to a 1 T applied field for a thin foil magnetized out of plane. While the data used in this analysis include that of Crangle *et al.* (see Fig. 3), we judge the uncertainty to be considerably greater than 0.1% based on the spread in the various data sets.

488 A similar analysis of the literature for nickel is shown in Fig. 5. As for Fe,
 489 the Ni data were fit to the Pauthenet parameterization with an additional
 490 term of a/H_{int}^2 . Each of the four data sets were fit independently in M_0 and a
 491 with a being constrained to be 0 or less as before. The only exception to this
 492 parameterization was the Crangle data set where a was fixed at 0 since there
 493 were no low field data to guide the fit. The fits are shown in Fig. 6. The
 494 “Average” parameterization curve was formed using the average M_0 and a
 495 from the fits. This average parameterization along with a proposed system-
 496 atic error band of $\pm 0.2\%$ or 0.11 emu/g is shown in Fig.6. Using 0.6179 T
 497 for the magnetic saturation induction of nickel and a demagnetization fac-
 498 tor of unity for a thin foil magnetized out of plane, makes the internal field
 499 0.6179 T less than the applied field near saturation. Thus a uniform external
 500 2 T magnetic field corresponds to an internal field of approximately 1.38 T.
 501 Over the range of H_{int} from 6 to 20 kOe (approximately 1.2 to 2.6 T applied
 502 field for a thin Ni foil magnetized out of plane normal to the surface) the
 503 following polynomial precisely follows the fit parameterization curve:

$$M_{\text{sat}}^{(\text{Ni})}(\text{emu/g}) = 55.063 + 1.5718 \times 10^{-2} H_{\text{int}} - 1.9678 \times 10^{-4} H_{\text{int}}^2, \quad (11)$$

504 with H_{int} in units of kOe. Converting Eq. 11 to applied field B_{app} in Tesla
 505 for the specific case of a thin Ni foil magnetized out of plane:

$$M_{\text{sat}}^{(\text{Ni})}(\text{emu/g}) = 54.959 + 0.181495 B_{\text{app}} - 0.019678 B_{\text{app}}^2. \quad (12)$$

506 This gives the magnetization per gram for nickel at 294 K with an applied
 507 field of 2 T as $M_{\text{sat}}^{(\text{Ni})} = 55.24 \pm 0.11$ emu/g. This translates into $0.5806 \pm$
 508 $0.0012 \mu_B/\text{atom}$

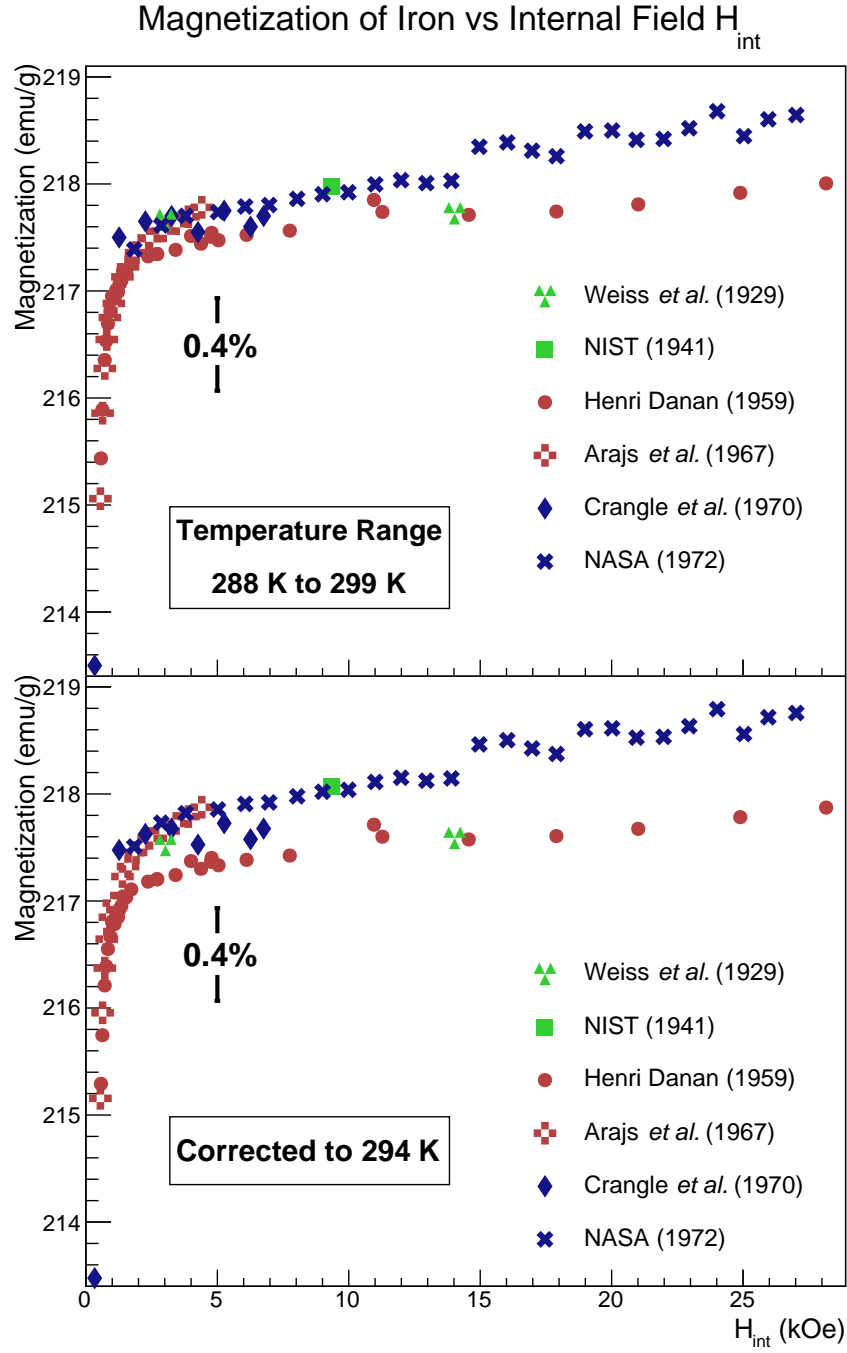


Figure 3: Published magnetization data from various sources for Fe shown versus internal field. The top plot shows the data for the temperature at which it was taken and the the bottom plot shows the same data corrected to 294 K. Note that zero is suppressed on the vertical axis. Refer to Table 2 for details on the data sets.

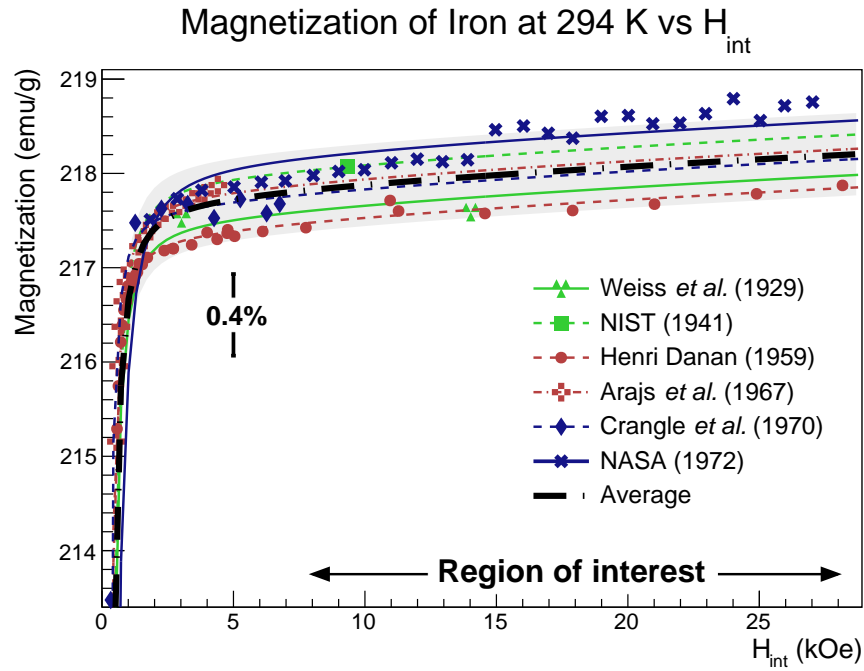


Figure 4: Published magnetization data from various sources for Fe plotted versus internal field corrected to 294 K. Magnetization data are fit using a modified form of Eq. 9 from [12]. Each of the six datasets are fit individually and the resulting curve fits averaged (see text for details). The error band corresponds to $\pm 0.20\%$ or ~ 0.44 emu/g.

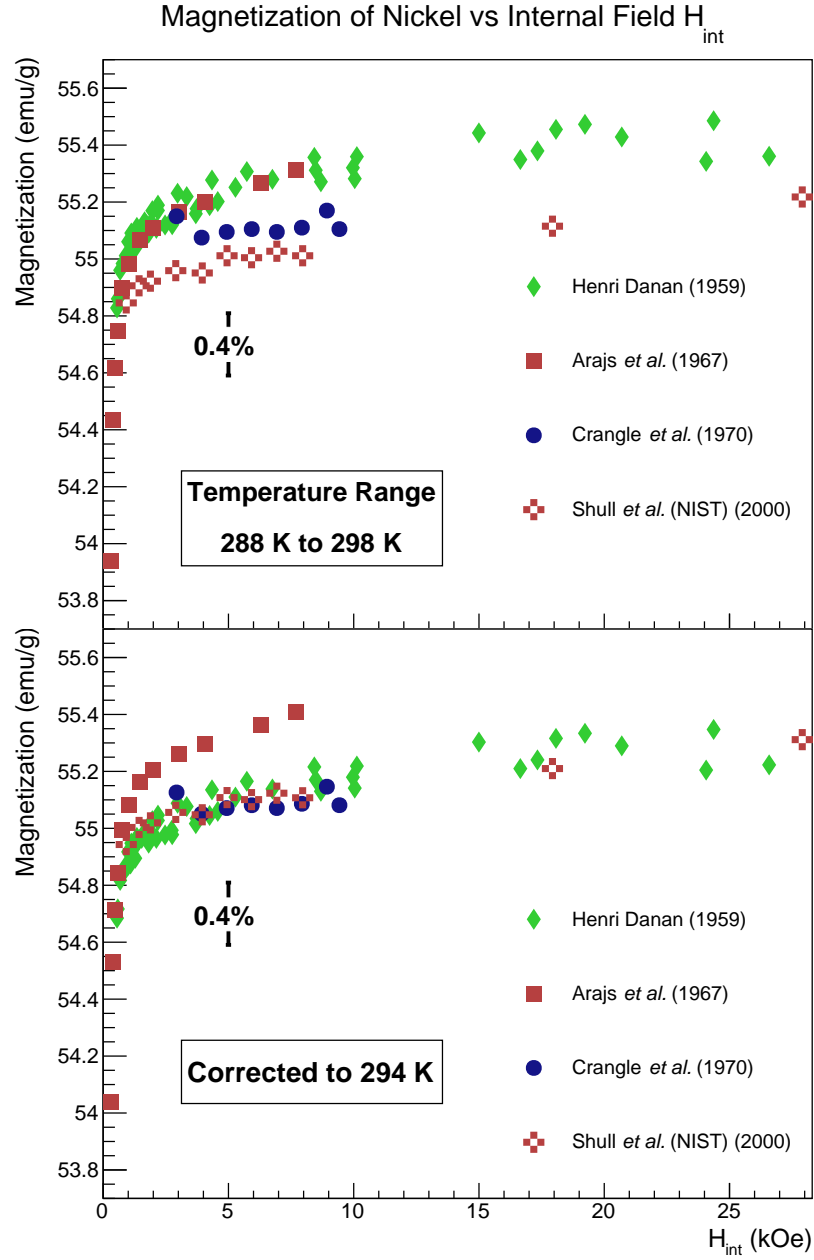


Figure 5: Published magnetization data from various sources for Ni shown versus internal field. The top plot shows data for temperature at which it was taken and the bottom plot shows the same data corrected to 294 K. There is good agreement in the data with the clear exception of that from Arajs *et al.* which are systematically higher by $\sim 0.5\%$. The reason for this discrepancy is not clear. Their publication claims $\pm 0.2\%$ accuracy for saturation magnetization which cannot explain the full difference.

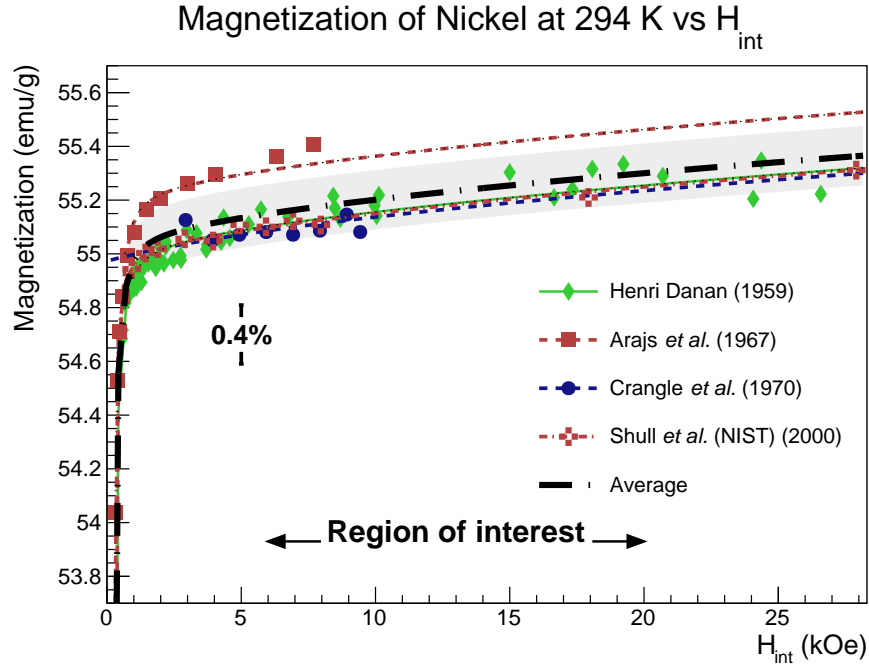


Figure 6: Published magnetization data from various sources for Ni plotted versus internal field corrected to 294 K and shown with proposed parametrization curve for internal fields up to 20 kOe (2 T). Magnetization data are fit using a modified form of Eq. 9 from [12]. Each of the six datasets are fit individually and the resulting curve fits averaged (see text for details). The error band corresponds to $\pm 0.20\%$ or ~ 0.11 emu/g.

509 2.1.4. Magnetocrystalline anisotropy

510 As previously discussed in section 2.1.2, the crystal structure of ferromag-
511 netic elements creates axes along which it is easier or harder to magnetize the
512 material. The origin of this anisotropy is primarily from the spin-orbit cou-
513 pling. The spin-spin coupling works to align adjacent spins in either parallel
514 or anti-parallel orientations but does not couple to the crystal lattice. The
515 spin-spin coupling can be rotated relatively easily with external magnetic
516 fields. Conversely, the orbital magnetic moments are strongly coupled to the
517 crystal lattice such that even very strong magnetic fields do not easily rotate
518 them. The coupling between the spin and orbital motion of each electron
519 tends to align the spins of the electrons along the crystal lattice such that
520 there is an additional energy associated with rotating the spins away from
521 what is termed the “easy axis” of the crystal. This coupling is also relatively
522 weak with fields of a few hundred oersteds being sufficient to overcome it.
523 For a more detailed discussion refer to *An Introduction to Magnetic Materials*
524 by Cullity and Graham section 7.4[30].

525 Iron and nickel (iron is body-centered cubic and nickel is face-centered
526 cubic) have hard, medium and easy magnetization axes due to their crys-
527 tal lattice structure. Magnetization along any axis other than the easy axis
528 requires a larger applied magnetic field due to the anisotropy energy. The
529 plots in Fig. 7 show typical magnetization curves for iron and nickel along
530 each of their magnetocrystalline axes. It is important to note that each of
531 the magnetization curves in Fig. 7 appears to approach the same saturation
532 magnetization. Pauthenet measured the saturation magnetization with pre-
533 cision along the different crystallographic axes for Ni and Fe and concluded
534 that the saturation magnetization is the same to within 0.01% at an internal
535 field of 10 kOe or greater[15].

536 2.1.5. Discussion of cobalt as a potential target material

537 Two key features of cobalt make it unfit as a precision target material.
538 First, the crystal structure of cobalt (mainly close-packed hexagonal at room
539 temperature) creates a greater magnetocrystalline anisotropy than it does for
540 the other two ferromagnetic elements. Pauthenet measured the difference in
541 saturation magnetization along the different axes to be at the 0.5% level
542 in his careful study of magnetization versus field[15]. In a polycrystalline
543 sample such as a foil that might be utilized in the Møller polarimeter, it is
544 not apparent how to determine the saturation magnetization.

545 Second, the crystal structure of cobalt changes from primarily close-

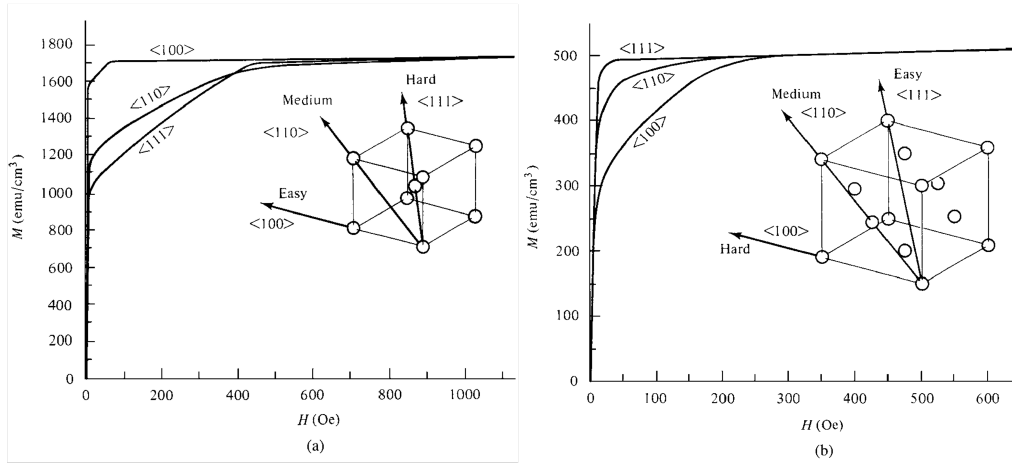


Figure 7: Magnetization curves for single crystals of Fe (a) and Ni (b) demonstrating the relative difficulty of magnetizing the crystals along different directions. (Figure adapted from [30].)

546 packed hexagonal below 690 K to face-centered cubic above this temperature.
 547 Near room temperature, a mixture of the two crystal structures generally of
 548 which the fractional composition varies from sample to sample producing a
 549 large uncertainty in the saturation magnetization for this material[31]. For
 550 these reasons, we have discarded cobalt as a candidate precision target ma-
 551 terial.

2.1.6. Target heating and temperature corrections

The magnetization of Fe and Ni is found for room temperature; however, there is a relatively large temperature-dependent correction ($\sim 1.5\%$ from liquid helium to room temperature for Fe) to the saturation magnetization as discussed in section 2.1.1. We now discuss the temperature corrections to the target magnetization for temperatures above 294 K that would be created by heating of the target by the electron beam. Note that although the following analysis is specific to the Hall A setup (circular foil, circular electron beam centered on the foil, un-rastered Gaussian profile electron beam). Further details of the calculation that allow it to be extended beyond these specific parameters can be found in [32].

When the electron beam is on target during a Møller polarimetry measurement, energy deposition causes the foil to heat up by a few degrees under usual conditions. Since there is a slight temperature dependence to the magnetization a correction will have to be applied. The further from the Curie temperature of the material, the smaller the correction will be. Therefore, we can expect the beam heating correction for Ni to be fractionally larger than that of Fe (see Table 1).

In the absence of a direct way of determining the temperature of the foil at the beam spot during operation or of monitoring the relative magnetization *in situ*, an estimate of the temperature increase must be made. This section provides a calculation of the foil heating from the electron beam under a set of assumptions.

The thin foil circular disks used in the Møller polarimeter are a few microns thick (see Fig. 8). The electron beam flux profile is approximately Gaussian with a typical 1σ radius of $100\ \mu\text{m}$.

The beam is approximately centered on the Møller target and has a natural helicity-correlated jitter of a few tens of microns. We calculate the approximate foil temperature change based on a few reasonable assumptions. We assume the beam introduces a heat load that is approximately a circular Gaussian distribution centered on the foil disk and that radiative black-body

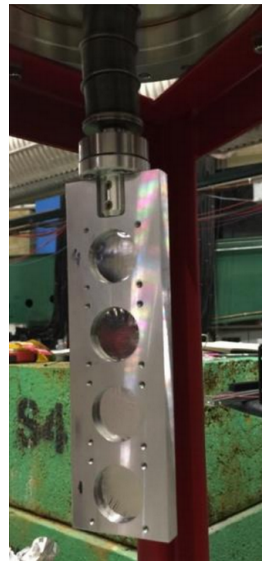


Figure 8: Target ladder with four thin iron foil disks. The support structure is aluminum.

589 cooling is negligible. We also assume that the aluminum frame constitutes
 590 an approximately infinite heat sink i.e. the temperature of the aluminum
 591 frame remains at or near room temperature, and that the foils are 0.65 inch
 592 in diameter and in perfect thermal contact with the aluminum frame along
 593 their edges.

594 The heat equation for this situation with only radial dependence and in
 595 the steady state is given as

$$\kappa \nabla^2 T = -\rho \alpha B_{\text{flux}}, \quad (13)$$

596 which reduces to

$$\frac{\partial}{\partial r} \left(r \frac{\partial T}{\partial r} \right) = -\frac{\rho \alpha}{\kappa} r B_{\text{flux}}, \quad (14)$$

597 where κ is the temperature dependent thermal conductivity of Fe; $\rho =$
 598 7.874 g/cm^3 is the density of Fe; α is the collision stopping power for elec-
 599 trons in Fe, which is a function of electron energy; and $B_{\text{flux}} = \frac{d^3 N_e}{ds dt}$ is the flux
 600 density of the beam in $e^-/(\text{cm}^2 \text{ s})$. This equation can be easily solved nu-
 601 merically with a Gaussian beam profile B_{flux} proportional to $e^{-r^2/2r_b^2}$, where
 602 r_b is the 1σ radius of the beam. The solution is shown in Fig. 9 with a
 603 $1 \mu\text{A}$ beam heat load with a typical spot size of $r_b = 100 \mu\text{m}$. Fig. 10 shows
 604 the dependence of the average temperature rise on the beam spot size for
 605 otherwise similar parameters. Using these data we obtained a temperature
 606 rise of $13.0^\circ\text{C}/\mu\text{A}$ for Fe as shown in Fig. 9. A similar temperature rise of
 607 $13.2^\circ\text{C}/\mu\text{A}$ was found for Ni foil. An ANSYS-Fluent simulation of heating
 608 for Fe foils under similar assumptions was found to agree at the 0.1°C with
 609 the temperature rise calculation detailed here or a $1 \mu\text{A}$ heat load on a $10 \mu\text{m}$
 610 thick foil.

611 The temperature dependence of magnetization for iron and nickel from
 612 [12, 15] yields the sensitivity shown in Fig. 11. The model was evaluated
 613 for applied fields of 2 T for nickel and 4 T for iron. A linear fit yields
 614 correction slopes of $-0.025 \text{ (emu/g/}^\circ\text{C)}$ for Ni and $-0.024 \text{ (emu/g/}^\circ\text{C)}$ for Fe.
 615 A conservative uncertainty of 30% is sufficient to cover both the uncertainties
 616 from the calculation of temperature increase and the magnetization versus
 617 temperature correction slope, yielding an uncertainty in the magnetization
 618 of $\pm 0.09 \text{ (emu/g}/\mu\text{A)}$ for both Ni and Fe.

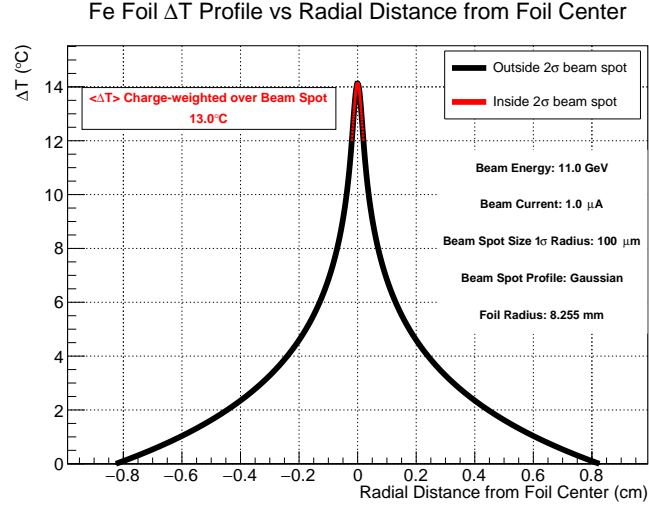


Figure 9: Foil temperature distribution in a 0.65 inch diameter foil under a $1 \mu\text{A}$ beam load. The electron beam is assumed to have a Gaussian distribution with a beam current and energy, foil radius and 1σ beam radius given in the plot. The red tip of the distribution is the part of the foil inside the 2σ beam spot. The average temperature rise weighted by the beam distribution over the beam spot is also shown. The ROOT macro for making this plot is called “FeFoilHeating.C” and is available at the following Git repository: <https://github.com/jonesdc76/MollerPolarimetry/blob/master/TargetPolarization/>

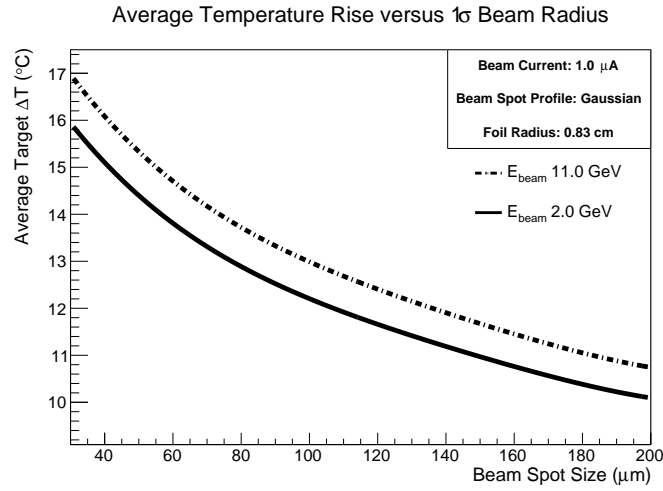


Figure 10: Average foil temperature increase (weighted by the beam charge distribution) shown versus beam spot size radius for the parameters shown.

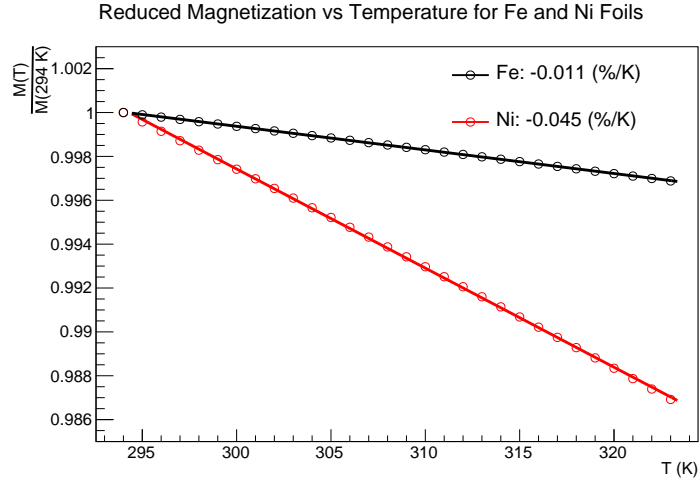


Figure 11: Magnetization versus temperature as a fraction of its value at 294 K from the parameterization in [12, 15] and evaluated at an applied field of 2 T for an Ni foil and 4 T for Fe. The fractional temperature correction given by model is shown as a linear fit and is $-0.011\%/K$ (-0.024 emu/g K) for Fe and $-0.045\%/K$ (-0.025 emu/g K) for Ni.

2.1.7. Effect of impurities

We next consider the effect of impurities on the measured magnetization. The experiments whose data are used in this analysis (with the possible exception of the measurement at NASA by Behrendt *et al.*) utilized highly pure Fe and Ni samples. Table 3 lists the level of impurities in the samples used in the various experiments whose data are used in this analysis. Although Weiss and Forrer [23] do not give a numerical value for the level of impurities they assure us that there were no impurities at a measurable level. They used this highly pure sample for the most precise results and many samples of less pure iron for less accurate studies. To set the scale, their less pure sample had a total of 0.22% impurities with 0.09% of that being carbon. Although the NASA measurement by Behrendt *et al.* does not list a purity level for the sample, we retain this measurement in spite of this uncertainty since it is only the second data set we found with precision measurements in the high field region (4 T applied fields) where we are typically running. An appropriately large systematic error is assigned in the end to account for this uncertainty.

Addition of non-ferromagnetic impurities typically decreases the magnetization (see for example [36, 37, 24]). Sanford *et al.* corrected for the effect of $\sim 0.01\%$ impurities which yielded a correction at the $\sim 0.02\%$ level[24]. Ahern *et al.* also found that adding copper to nickel reduced the magnetization by about 2% for every 1% of the nickel replaced by copper. If we set the uncertainty from impurities at twice the fractional level of impurities, the largest error (0.12%) comes from the ARAJS and Dunmyre data on iron. Given the purity of the Fe and Ni samples used, we assign no additional systematic error beyond that already determined from the spread in the data. We will revisit the effects of impurities once again in the determination of the spin component of the magnetization.

Another source of impurities generally not accounted for in assays is the surface oxidation. Iron oxides such as Fe_3O_4 , have a much smaller magnetization than pure Fe. Alex Gray's group at Temple University took XMCD measurements for us at the Advanced Light Source on a pure Fe foil which we provided from our Møller target materials. These measurements, which probe the material surface to a depth of a few nanometers, showed clear evidence of surface oxidation in spite of their highly specular appearance. This suggests that foils nearing micron level thickness could have surface contamination from oxides at the 0.1% level. We expect that using clean foils with

Table 3: Level of impurities from the various measurements used in this analysis. Note that Danan used the same Fe sample measured by Weiss and Forrer. Crangle and Goodman used two samples for Fe and two for Ni of differing purities.

Experiment	Element	Impurity Fraction
Weiss and Forrer [23]	Fe	“No detectable impurities”
R. Sanford <i>et al.</i> (NIST)[24]	Fe	<0.01%
H. Danan [25, 21]	Fe	Same as Weiss and Forrer
Arajs and Dunmyre [33][26]	Fe	~600 ppm
Crangle and Goodman [20]	Fe	0.06% and 0.006%
Behrendt and Hegland (NASA)[27]	Fe	Not given
H. Danan [25, 21]	Ni	0.01%
Arajs and Dunmyre [34, 35, 26]	Ni	~30 ppm
Crangle and Goodman [20]	Ni	0.05% and 0.005%
R. Shull <i>et al.</i> (NIST)	Ni	10 ppm

no surface oxidation apparent to the naked eye and with a thickness of 10 μm will render this source of uncertainty negligible at the $\ll 0.1\%$ level.

2.1.8. Nuclear contribution to the magnetic moment

Discussion of the nuclear contribution to the magnetic moment appears to be absent from the literature on magnetization measurements. This is most likely due to the suppression of the nuclear magneton relative to the Bohr magneton by the electron to proton mass ratio ($\mu_B/\mu_N = m_p/m_e$), a factor of about 1/2000. However, in the determination of target polarization for the Møller polarimeter, effects at the 0.1% level require consideration. In the nucleus spins are paired in such a way that all even-even nuclei have zero spin. Fortunately, the isotopic distribution of iron (26 protons) is such that 97.9% of natural iron is from even-even isotopes. The single even-odd naturally occurring isotope ^{57}Fe has a negligible nuclear spin of $0.09\mu_N$ [38]. For nickel (28 protons) the situation is also favorable with natural nickel being composed of 98.9% even-even isotopes. This gives us another two orders of magnitude suppression and renders the nuclear spin contribution completely negligible. However, for cobalt (27 protons), the only stable isotope has a nuclear spin of $4.63\mu_N$, potentially creating errors at the 0.2% level and adding another reason not to use Co foil.

675 2.1.9. Defects from target irradiation

676 Another potential source of systematic error in determining target satura-
677 tion magnetization is the effect of radiation damage. If a sufficient fraction of
678 lattice sites are dislodged/damaged this could potentially change the target
679 saturation polarization. We estimated the radiation damage by integrating
680 the Mott scattering cross section from momentum transfer of infinity down
681 to the threshold set by the permanent lattice displacement energy (nuclear
682 recoil energy of 40 eV) weighting the cross section by the number of addi-
683 tional atoms that are dislodged by the initial atom using the NRT method
684 to estimate the displacements per atom [39]. This produced a total cross
685 section of order 100 barns. While this effective displacement cross section is
686 relatively large, it would take more than 100 years in our typical 1 μ A beam
687 for a significant fraction of the target lattice sites to be displaced. This is
688 consistent with non-observation (to the best of our knowledge) of such an
689 effect in any Møller polarimeter worldwide. Given that we have not observed
690 such an effect directly at Jefferson Lab in our extensive use of precision Møller
691 polarimeters in both Halls A and C, and that our order of magnitude esti-
692 mate suggests insignificant fractional damage, we have chosen not to add an
693 additional systematic error to account for radiation damage.

694 2.2. Determination of g' and the spin component of magnetization

695 Magnetization arises from a combination of spin and orbital contribu-
696 tions. In ferromagnetic materials, the orbital component is suppressed or
697 “quenched” compared to the spin. To find the spin polarization of the target
698 foils we must determine the spin fraction of the magnetization. The spin
699 component of the magnetization can be determined from measurements of
700 g' , the total g-factor for atomic electrons which can be obtained from magne-
701 tomechanical experiments utilizing the Einstein-de Haas effect or the Barnett
702 effect.³ In general, the g -factor is related to the gyromagnetic ratio γ of a
703 charged body as

$$\gamma = g \frac{\mu_B}{\hbar}, \quad (15)$$

³The Einstein-de Haas effect (rotation by magnetization) is the rotation of a macroscopic body in a magnetic field when the field is reversed[40, 41]. The Barnett effect (magnetization by rotation) is the converse, the production of a magnetic field by rotation of a macroscopic body[42, 43].

704 where μ_B is the Bohr magneton.⁴ The electron has two g -factors which we
 705 refer to as $g_S \approx 2$ for its spin, and $g_L = 1$ for its orbital motion. For atoms
 706 having both orbital and spin angular momentum, g' is a linear combination
 707 of g_S and g_L , which is not known *a priori* and must be determined from
 708 measurement.

709 In publications from the early to middle 1900s, g_S was assumed to be
 710 exactly 2 where we now know it to be (up to a sign) the most precisely
 711 measured scientific constant $g_S = 2.00231930436256(35)$. In most cases, this
 712 0.1% difference is not consequential, but for the level of precision we are
 713 trying to reach, this is not negligible and care must be taken to track down
 714 wherever 2 has been substituted for g_S .

715 The relationship of g' to the magnetic moment contribution is often given
 716 in the literature following the example of Kittel[44] in the following form:
 717 [45, 46]

$$g' = \frac{2(M_S + M_L)}{M_S + 2M_L} = \frac{2M_{\text{tot}}}{M_{\text{tot}} + M_L}, \quad (16)$$

718 where M_{tot} is the total magnetization. M_L and M_S are the components of
 719 magnetization arising from orbital and spin magnetic moments respectively.
 720 This expression immediately leads to the expression of orbital and spin con-
 721 tributions to the magnetic moment as [3]

$$\frac{M_L}{M_{\text{tot}}} = \frac{2 - g'}{g'}, \quad \frac{M_S}{M_{\text{tot}}} = 1 - \frac{M_L}{M_{\text{tot}}}. \quad (17)$$

722 The gyromagnetic ratio, γ is defined as the ratio of the magnetic moment
 723 of a particle or body to its angular momentum. In measurements of g' where
 724 magnetization and angular momentum of macroscopic bodies are directly
 725 measured, the gyromagnetic ratio is determined as

$$\gamma = \frac{M}{J},$$

726 where M and J are the projections of \mathbf{M} and \mathbf{J} along the direction of mag-
 727 netization. We can divide these into their spin and orbital components:

$$M = M_L + M_S, \quad J = J_L + J_S,$$

⁴In early publications sometimes the gyromagnetic ratio is given as $\rho = L/M$ the ratio of the angular momentum to the magnetic moment where at other times it is defined in the usual way as the reciprocal $\gamma = 1/\rho = M/L$.

where the subscripts L and S refer to orbital and spin respectively. At the atomic level the magnetic moment \mathbf{M} is related to the orbital and spin angular momentum as $\mathbf{M}_S = g_S \mu_B \mathbf{S}/\hbar$ and $\mathbf{M}_L = g_L \mu_B \mathbf{L}/\hbar$, such that a unit of spin angular momentum yields g_S/g_L more magnetic moment than a unit of orbital angular momentum. This holds also at the macroscopic level so that we can write

$$\gamma = g' \frac{\mu_B}{\hbar}, \quad g' = \frac{M_{\text{tot}}}{M_S/g_S + M_L/g_L}. \quad (18)$$

To high precision $g_L = 1$ yielding ⁵

$$g' = \frac{M_{\text{tot}}}{M_S/g_S + M_L} = \frac{g_S M_{\text{tot}}}{M_S + g_S M_L}. \quad (19)$$

from which we recover Eq. 16 if we substitute $g_S = 2$. Eq. 19 is the exact form which should be used in this analysis. Furthermore, the exact form of Eq. 17 is the slightly more complicated

$$\frac{M_L}{M_{\text{tot}}} = \frac{g_S - g'}{g'(g_S - 1)}. \quad (20)$$

This gives for the spin component

$$\frac{M_S}{M_{\text{tot}}} = 1 - \frac{M_L}{M_{\text{tot}}} = \frac{g_S(g' - 1)}{g'(g_S - 1)}, \quad (21)$$

which decreases the spin contribution to the total magnetization compared to Eq. 17 by 0.11%.

2.2.1. g' for Fe

The most precise measurements of g' come from measurements of the gyromagnetic ratio of iron using the Einstein-de Haas effect. These magnetomechanical experiments are highly elaborate requiring high precision to observe the tiny effects of interest. The Einstein-de Haas experiments are simple in principle: a sample is suspended from a torsion pendulum along the axis of

⁵There is a small correction to g_L that arises from the finite mass of the nucleus at the order of the ratio of the electron mass to that of the nucleus ($\sim 1 \times 10^{-5}$) [47]. This is two orders of magnitude below the correction considered here of $(g_S - 2)/g_S$ and will be neglected.

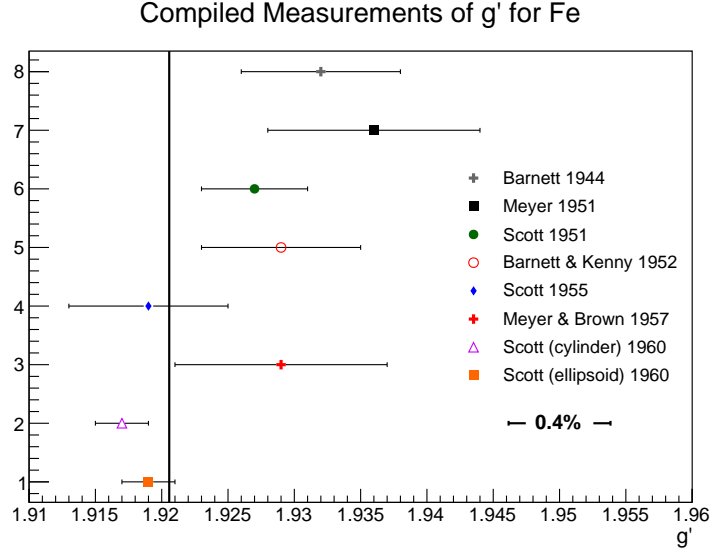


Figure 12: Values of g' for iron as determined by various experiments between 1940 and 1960. The naive constant fit to these data is given by the vertical black line whose value is $g' = 1.9206$.

747 a magnetic field. Upon reversal of the field a small torque on the sample is
748 measured primarily due to reversal of the valence electron spins. In practice,
749 these experiments are highly technical since the torques on the sample from
750 the Earth's magnetic field can be 7-8 orders of magnitude larger than the
751 torques from spin reversal[41]. Elaborate coil setups were utilized to cancel
752 the Earth's field along with any stray magnetic fields in the region and iso-
753 lation systems incorporated to keep the sample free from interference from
754 outside vibrations. The gyromagnetic ratio was then determined from the
755 measured ratio of the angular momentum to the magnetic moment. Similarly
756 complex systems were used in the experiments which measured the Barnett
757 effect. In these experiments a relatively large sample was rotated and the
758 change in magnetic flux measured in a system of pickup coils.

759 A compilation of g' measurements on iron from magnetomechanical ex-
760 periments is shown in Fig. 12. These data were taken from compilations in
761 two papers⁶ by G. Scott in 1962[41] and Meyer and Asch in 1961[45]. For ref-

⁶There are two inconsistencies between these references[41, 45]. 1. Table 1 of [45] has Barnett 1941 $\rho e/mc = 1.035$ ($g' = 1.932$) which comes from averaging measurements using

762 erence, the data included in these compilations comes from [43, 48, 49, 50, 51].
763 The final two measurements done by G. Scott are by far the most precise.
764 It is clear given the fit probability of 0.004 and from discussions of how the
765 uncertainties were determined, that the error bars do not in all cases reflect
766 the actual systematic error, which, in at least some of the measurements,
767 is underestimated. The most accurate measurements were made by Scott,
768 who without stated justification, concludes that his most recent measure-
769 ment of $g' = 1.919 \pm 0.002$ on a prolate ellipsoid sample is the best value
770 to use for iron [51, 41] even though he measured $g' = 1.917 \pm 0.002$ on a
771 cylindrical sample using the same apparatus. It is likely that he regarded
772 the ellipsoid-shaped sample more accurate because of the uniformity of the
773 internal magnetic field this shape produces. It is worth noting that his latest
774 value $g' = 1.919$ appears to be the value taken as standard in the literature
775 (see for example [52, 53]). It not clear what systematics may be at play here
776 (sample purity, shape, porosity, preparation/annealing process).

777 For the three samples used in the measurements g' of Fe, the sample
778 purities were as follows:

- 779 • Scott cylinder 99.94% with primary impurities O(0.04%), C(0.005%),
780 N(0.004%), S(0.003%) and Ni(0.0015%) [48]
- 781 • Scott ellipsoid, 99.89% with primary impurities Ni(0.05%), Si(0.01%),
782 O(0.005%), Co(0.005%) [51]
- 783 • Meyer 1957, 99.9% with primary impurities Mn(0.042%), S(0.029%),
784 Si(0.02%) [50]

785 Scott carefully measured the effect of mixing the ferromagnetic elements
786 Fe, Co and Ni and since their g' values are all within 5% of each other trace
787 amounts of impurities ($<1\%$) from of Ni and Co in Fe will have negligible
788 effect on the value of g' (see Fig 1 of [54]). There is little guidance in the
789 literature for the effect of trace amounts of O, Mn, N, C and S on g' for
790 Fe making it difficult to set the scale for such errors. However, Ladislav
791 Pust *et al.* found very little difference in the related quantity spectroscopic

the Einstein-de Haas and Barnett effects. Scott seems to only use Barnett's measurements of the Einstein-de Haas effect and quotes Barnett's measurement as $g' = 1.938$. We retain Barnett's average of the two methods. 2. Scott [41] gives Meyer's 1957 value for Fe as $g'=1.932$, whereas Meyer [45] uses 1.929. We use Meyer's value.

792 g between pure Fe and that with 3% Si by weight[55]. We will see in the
 793 coming paragraphs that the spectroscopic g -factor is inversely related to g'
 794 such that if one increases, the other decreases and vice versa.

795 An error-weighted fit to these data gives a result of 1.9206 ± 0.0012 . How-
 796 ever, the χ^2/NDF is 2.41 indicating that systematic errors have been under-
 797 estimated. Following the example of the Particle Data Group (see Sec. 5.2.2
 798 of [56]), and inflating each of the error bars by $\sqrt{\chi^2/\text{NDF}} = 1.553$ to give a
 799 χ^2/NDF of unity (p-value = 0.43) yields an error of 0.0019 or $\pm 0.10\%$.

800 Related to g' is the spectroscopic g -factor often referred to as g from
 801 ferromagnetic resonance (FMR) experiments⁷. FMR works by placing a fer-
 802 romagnetic sample in a resonant microwave cavity. The cavity is placed in a
 803 uniform magnetic field at right angles to the direction of propagation of the
 804 microwaves. A microwave source feeds the cavity and a detector monitors the
 805 energy coming out of the cavity. When the magnetic field is turned on, the
 806 magnetic moments of the atoms will begin to precess around the direction
 807 of the applied magnetic field with a frequency that depends on the effective
 808 magnetic field H_{eff} and the g -factor of the sample material as follows:

$$\hbar\omega = g\mu_B H_{\text{eff}} \quad (22)$$

809 where H_{eff} , the effective magnetic field depends on the applied magnetic
 810 field strength as well as the magnetization, shape and relative alignment of
 811 the specimen (see [44, 46] for a more detailed explanation). The magnetic
 812 field strength is then swept over a range until the resonance condition is
 813 met where the precession frequency matches that of the microwave cavity.
 814 At resonance a drop in power exiting the cavity will be observed due to
 815 the energy being absorbed by the sample. Spectroscopic g is determined by
 816 measuring the magnetic field which excites this resonance. For a time it was
 817 thought that spectroscopic g and g' were the same i.e. that spectroscopic
 818 and magnetomechanical experiments were measuring the same g -factor until
 819 Kittel (1949)[44] and Van Vleck (1950)[57] independently showed that these
 820 are related but not identical quantities. In the case of spectroscopic g , the
 821 lattice momentum offsets the intrinsic orbital momentum so that the total
 822 angular momentum is approximately equal to the spin contribution[44, 58].

⁷For a simple explanation of FMR see <http://www.physik.fu-berlin.de/einrichtungen/ag/ag-kuch/research/techniques/fmr/index.html>

823 Therefore, spectroscopic g is given by

$$g \left(\frac{\mu_B}{\hbar} \right) = \frac{M_L + M_S}{S}, \quad (23)$$

824 where S is the electron spin. To a good approximation it can be shown
 825 that $g = \frac{2M_{\text{tot}}}{M_{\text{tot}} - M_L}$ where g' is given approximately by Eq. 16. Thus, the
 826 orbital component increases the magnitude of g and decreases g' . Using
 827 these equations we can easily derive what is known as the Kittel-Van Vleck
 828 relationship

$$\frac{1}{g} + \frac{1}{g'} = 1. \quad (24)$$

829 Although this relationship is approximate and should not be considered
 830 valid below the $\pm 0.1\%$ level, it has been shown to work quite well in the
 831 literature (see for example Fig. 1 of [45]). Therefore, we can utilize spectro-
 832 scopic measurements of g to further check our value of g' . Figure 13 shows
 833 a compilation of measurements of g for iron. A simple error-weighted fit to
 834 these data gives a value of $g = 2.086 \pm 0.004$. Using Eq. 24 gives $g' = 1.921$
 835 in precise agreement with the error weight fit to g' from magnetomechanical
 836 experiments. While we cannot place the same confidence in this derived
 837 value of g' as the direct measurements, it is reassuring that determinations
 838 from completely different techniques appear to be consistent.

839 **Recommendation for Fe:** In light of these findings we recommend
 840 using the value of the simple error-weighted fit with an inflated systematic
 841 error to reflect the tension in the world data: $g' = 1.9206 \pm 0.0019$. The
 842 0.0019 error comes from inflating the error reported by the fit by 55.3%
 843 which is required to remove the tension in the data and give a χ^2/NDF of
 844 1. The systematic error from impurities is assumed to be included in this
 845 uncertainty. This choice places Scott's recommended value of $g' = 1.919 \pm$
 846 0.002 measured on an ellipsoid Fe sample [41] comfortably within 1σ but his
 847 earlier measurement on a cylindrical sample 1.9σ off.

848 2.2.2. g' for Ni

849 A number of measurements of g' for nickel were performed by A. J. Meyer
 850 *et al.*, G. G. Scott *et al.* and S. Barnett *et al.* during the 1950's. At first
 851 there were striking differences in the values found for nickel ranging from
 852 1.83 to >1.99 . Furthermore, the measurements of spectroscopic g from res-
 853 onance experiments gave a much lower value of g' using the Eq. 24. A
 854 couple of systematic errors in the measurement techniques of both Meyer

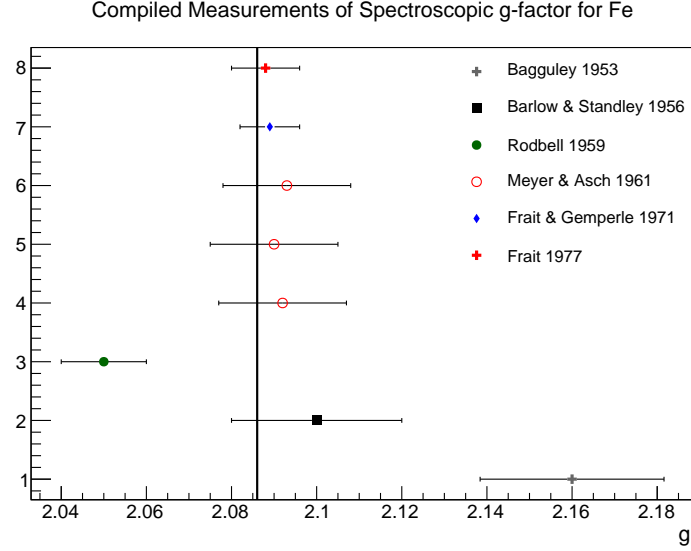


Figure 13: Values of spectroscopic g as determined by various experiments over two decades. The error-weighted fit to these data is given by the vertical black line whose value is $g = 2.086$.

and Scott were pointed out by Brown which brought the data into much better agreement[41]. However, a considerable inconsistency remained between the measurement of Barnett *et al.* and that of Scott and Meyer. Barnett determined $g' \approx 1.91$ compared to the 4% lower $g' \approx 1.84$ found by Meyer and Scott[45, 41]. To investigate the possible reasons for this discrepancy, Meyer measured the Curie temperature and the saturation magnetization of the Ni samples used in each of the measurements. Whereas Scott and Meyer had used nearly pure Ni, Barnett's sample had 1.4% impurities. The presence of these impurities significantly changed the magnetic properties of his Ni sample such that the Curie temperature was reduced from 360°C for pure Ni to 285°C and the saturation magnetization increased from 58.90 to 71.04 (in units of abamp cm³/g)[41]. Scott concludes that this stark shift in magnetic properties makes Barnett's measurements "difficult to retain"[41]. However, this discrepancy provides evidence that the presence of certain impurities can have a significant effect on the measurement of g' .

Scott performed a series of four measurements on the same Ni sample in 1952, 1953, 1955 and 1960 and concluded that $g' = 1.835 \pm 0.002$ [41]. Meyer *et al.* also measured g' for different Ni samples in 1957 and 1958 finding

873 1.852 ± 0.009 and 1.845 ± 0.007 [45]. An error-weighted fit to these values gives
874 $g' = 1.8365 \pm 0.0019$ with a χ^2/NDF of 2.5.

875 The impurities in the samples used are as follows:

- 876 • Scott: 99.82% Ni with main impurities Si(0.1%), Fe(0.032%), Mn(0.030%),
877 and C(0.01%)[59]
- 878 • Meyer, 1957: 99.9% Ni with impurities not provided[50]
- 879 • Meyer, 1958: 99.99% with negligible impurities[45]

880 Looking at the impurities in Scott's sample, we can rule out the effects
881 of Fe and Mn as contributing significantly to a systematic offset using the
882 data in [60, 54]. With carbon impurities at 0.01% this can be considered
883 negligible. Meyer's analysis of the magnetic properties of the Ni sample used
884 by Scott showed that although the saturation magnetization was changed
885 insignificantly, the Curie temperature decreased by 11°C. Since we were not
886 able to locate data to calibrate the effect of Si impurities at 0.1% in Ni, a
887 similar approach to that used for the Fe data will be used here. Inflating
888 the error bars on each of the three data points by 1.581 gives a best fit of
889 $g' = 1.8365 \pm 0.0030$ with a p-value of 0.37.

890 Once again we can use measurements of the spectroscopic g -factor from
891 magnetic resonance experiments and Eq. 24 as an independent check of our
892 proposed value of g' . Table II. of Meyer and Asch [45] provided a compilation
893 of g -factors measured in magnetic resonance experiments and concluded that
894 for nickel $g = 2.185 \pm 0.010$ which translates into $g' = 1.844 \pm 0.008$ in good
895 agreement with our proposed value.

896 **Recommendation for Ni:** in light of these findings we recommend
897 using the value $g' = 1.8365 \pm 0.0030$ for nickel. The value comes from
898 an error-weighted fit to Scott's and Meyer's measured values after increas-
899 ing each of the error bars by 1.581 to accommodate for the underestimated
900 systematic uncertainty.

901 2.2.3. *Temperature dependence of g'*

902 The measurements of g' used in this analysis have all been at room tem-
903 perature which is not well-defined but is broadly accepted to be near 20°C
904 give or take a few degrees. Although the target foils in the Møller polarimeter
905 will generally be at room temperature, during measurements with a typical
906 1 μA of beam on target, the foils will heat up by 10-15 degrees Celsius as

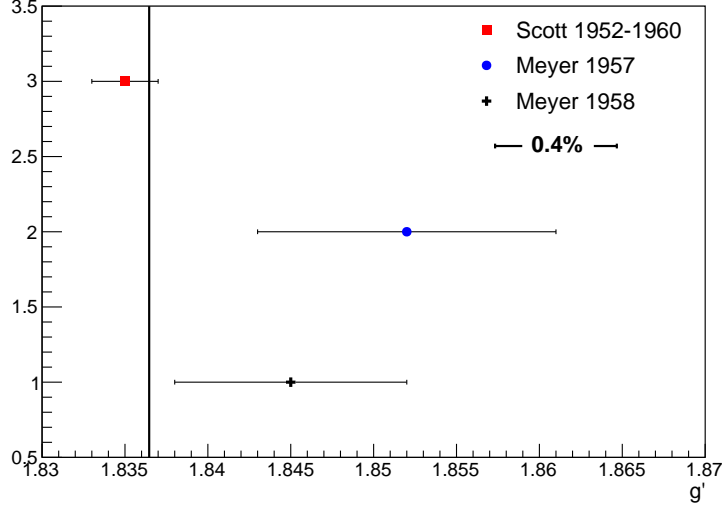


Figure 14: Values of g' for nickel as determined by various experiments between 1950 and 1960. The systematic error on Scott's value as proposed in the text is shown. The error-weighted fit to these data using the proposed error given by the vertical line is $g' = 1.8365 \pm 0.0036$.

we saw in section 2.1.6. This raises the question of whether or not the room temperature values of g' are sufficiently accurate during measurements at elevated temperatures.

The temperature dependence of saturation magnetization arising from spin waves was discussed in section 2.1.1. If this change in saturation magnetization results in a change of the fraction of magnetization arising from orbital and spin components, this would necessarily imply a change in g' . Conversely, a temperature-independent g' would imply that spin waves proportionately decrease both the orbital and spin components of magnetization.

In Kittel's 1949 paper on the relation of g and g' , he discusses the temperature dependence of g' and suggests there is not enough data to make conclusions[44]. Since then several measurements have been made of g across a broad temperature range for the ferromagnetic elements and alloys. These experiments, which measure g since it is a technically much easier measurement than g' , particularly with changing temperatures, are typically at the 1-2% precision level. However, a change in g indicates the inverse change in the g' by Eq. 24. A nice summary of these measurements is found in [61].

924 It is worth noting that in all cases where pure Ni and Fe were measured,
 925 the g -factor was always found to be constant within experimental errors,
 926 typically at the 1-2% level. However, for alloys, this is not always the case
 927 with variations of several percent being observed (see for example [62, 63]).

928 In two cases, extremely accurate measurements were made across a broad
 929 temperature range, one for pure Ni and the other for 97% Fe. The first
 930 of these was by G. Dewar *et al.* in 1977 on pure nickel foil of 20 μm
 931 thickness. They found $g = 2.187 \pm 0.005$ constant over the temperature
 932 range 20-364°C[64]. This constitutes a 0.23% test of temperature depen-
 933 dence over a range much larger than we care about. The second experi-
 934 ment in 1981 by Ladislav Pust and Zdenek Frait measured the g -factor of
 935 Fe-3wt%Si in the temperature range from 3.5 to 300 K to be constant at
 936 $g = 2.0793 \pm 0.0005$ [65]. The extreme accuracy of their measurement al-
 937 lowed them to probe the temperature dependence of g at the 0.02% level and
 938 they conclude that there is no evidence of temperature dependence across
 939 the temperature range they measured. The plot from their paper showing
 940 the measurement of g with temperature is shown in Fig. 15. A summary of
 941 the various measurements of g is provided in Table 4.

942 Thus, there is strong evidence that spectroscopic g and by extension g'
 943 are, in fact, highly constant for nickel and iron well below their Curie tem-
 944 peratures. This implies that the spin-wave correction does not significantly
 945 alter the fraction of magnetic moment arising from orbital and spin contribu-
 946 tions for these two ferromagnetic elements. We will revisit spin waves in the
 947 context of the field-dependence of g' , but we conclude that it is safe to pro-
 948 ceed with confidence using the room temperature measurements of g' with
 949 negligible error.

950 2.2.4. Magnetic field dependence of g'

951 In the 1950's while Scott was performing precise measurements of g' ,
 952 he initially found that g' decreased at very low fields and asymptotically
 953 approached a larger constant value at higher fields. He published three papers
 954 documenting the low-field behavior of g' for nickel and iron and alloys of the
 955 two [72, 59, 73]. In 1960, he found that this low-field behavior was due to
 956 a systematic error in his measurement technique[51]. After improving the
 957 technique and re-measuring, he concluded that, in fact, g' is independent of
 958 applied field for Ni and Fe over the range of fields he was measuring. His
 959 setup utilized a solenoid with a total area 78000 cm^2 which he energized
 960 with 1-16 mA producing fields as high as 40 gauss. Although these fields

Table 4: Results of experiments measuring the spectroscopic g -factor as a function of temperature for various ferromagnetic materials. Without exception all consider the g -factor to be constant within error.

Publication	Year	Material	g -factor	Temp. ($^{\circ}\text{C}$)
Frait <i>et al.</i> [65]	1981	Fe-3wt%Si	2.0793 ± 0.0005	-270 to 27
Haraldson <i>et al.</i> [66]	1981	Ni	2.20 ± 0.02	20 to 358
Gadsden <i>et al.</i> [62]	1978	Ni	2.20	-269 to 20
Dewar <i>et al.</i> [64]	1977	Ni	2.187 ± 0.005	20 to 364
Bastian <i>et al.</i> [67]	1976	Ni-Fe alloys	const. $\pm 1\%$	20 to >300
Rodbell [68]	1964	Ni	2.22 ± 0.03	-140 to 360
Rodbell [69]	1959	Fe	2.05 ± 0.01	-196 to 850
Standley <i>et al.</i> [60]	1955	Ni	2.17 - 2.18	20 to 200
Bagguley <i>et al.</i> [70]	1954	Ni	2.22 ± 0.02	20 to 600
Bloembergen [71]	1950	Ni	2.20 ± 1 - 2%	24 to 358

were sufficient to induce significant magnetization in the elongated samples, the high currents only induced magnetizations approaching half the level of saturation magnetization. Here we look at evidence to demonstrate that g' remains field-independent in the several tesla applied field region where the Møller polarimeter operates.

FMR measurements of spectroscopic g are taken with the sample at saturation magnetization where the magnetization is well-determined from the literature and the g -factor can be calculated (see Eq. 22). The frequency independence of the g -factor often tested in the literature is simultaneously a test of the magnetic field-dependence of g since the frequency is a function of the effective field, H_{eff} .

In 1971, Z. Frait and R. Gemperle measured the g -factor of single iron crystals across a range of frequencies from 12 to 70 GHz requiring a broad range of static magnetic fields[74] which roughly corresponds to applied fields from 0.08 T to 1.6 T (for details on converting between resonance frequency and applied field see Kittel[75]). They found that $g = 2.089 \pm 0.007$ and that it is frequency independent over this range within their experimental error ($\pm 0.33\%$). In 1977, Z. Frait published an FMR measurement of $g = 2.088 \pm 0.008$ for pure polycrystalline iron at three frequencies, 26 GHz (at 0.32 T), 36 GHz (at 0.57 T) and 70 GHz (at 1.53 T)[76]. Once again he concluded that

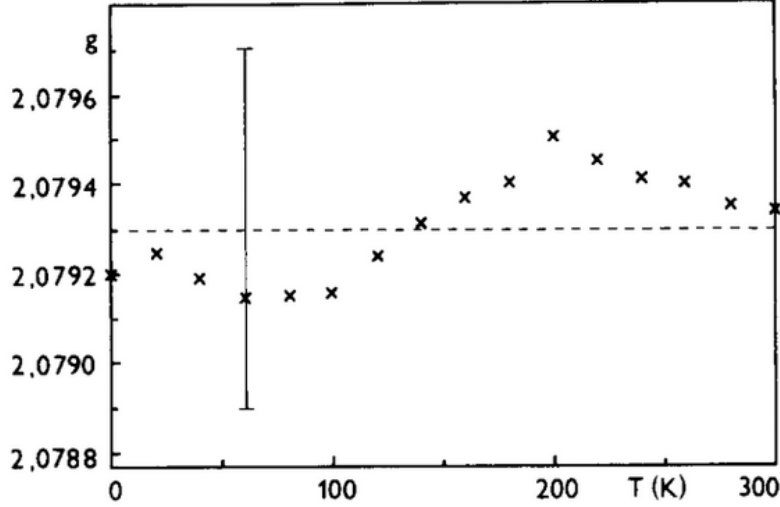


Figure 15: Plot of g -values vs. temperature taken from [65]. The vertical bar denotes the accuracy of these values (± 0.0004).

981 within experimental error this value is frequency independent, constituting
 982 a high-field test of field dependence on g for iron. Unfortunately, Pust *et al.*
 983 make no mention of frequency-dependence in their $\pm 0.024\%$ measurement
 984 of the g -factor of Fe-3wt%Si even though their results were averages of four
 985 different frequencies, 36 GHz, 70 GHz, 86 GHz and 95 GHz[65].

986 For nickel the data are less precise but point to the same conclusion that
 987 g is field-independent. In 1950 Bloembergen measured the g -factor of nickel
 988 to be 2.23 at 9.05 GHz with a field of 0.116 T and 2.24 at 22.44 GHz with
 989 a magnetic field of 0.54 T. These values are equal within the error of the
 990 experiment. In 1959, Rodbell found that for nickel g was constant at the
 991 0.5% level over a range of magnetic fields up to 0.3 T[69]. In 1965, Frait
 992 found that g was independent of frequency for pure nickel at the 2% level
 993 over a range of frequencies from 8.5 GHz to 72 GHz (roughly corresponding
 994 to applied fields of 0.1 T - 2.4 T). He also found that an alloy consisting of
 995 42% Fe and 58% Ni was independent of frequency over the same range at
 996 the 1% level[77]. Finally, as we saw earlier in section 2.2.3 the value of g'
 997 for nickel derived from high-field measurements of g agrees well within error
 998 with the direct measurements at low field, providing further evidence of the
 999 validity of the asymptotic value of g' for nickel.

1000 Although we found no field-dependence of g' for Fe and Ni in the liter-
1001 ature, the evidence is not sufficiently precise to rule out 0.1% level changes
1002 at high field. Given this consideration we chose to place an upper limit on
1003 the field dependence using measurements of high-field susceptibility as we
1004 outline next.

1005 Given that g' provides a measure of the fraction of the magnetization
1006 from orbital and spin contributions (see Eq. 20) any field dependence of g or
1007 g' is a signal that the fractional contribution from spin is field-dependent. In
1008 section 2.2.3, we concluded that the spin-wave correction did not significantly
1009 alter g' as evidenced from the temperature independence of g ; however, there
1010 are other field-dependent contributions to magnetization which can be sep-
1011 arated from the spin-wave contribution by either going to the high-field or
1012 low temperature regime where spin-wave contributions are negligible. The
1013 linear increase of magnetization with applied field in the high-field region is
1014 referred to as the high-field susceptibility $\chi_{\text{HF}}(H) = \partial M / \partial H$. χ_{HF} is com-
1015 posed of both orbital and spin contributions[78, 79, 11]. Some attempts have
1016 been made to calculate the relative contributions of the orbital and spin to
1017 the high-field susceptibility[80]. An upper limit on the field dependence of
1018 the spin fraction can be made by assigning the full high-field change in mag-
1019 netization solely to a spin or to an orbital contribution. Tables 5 and 6 list
1020 5 measurements of the high-field susceptibility for Fe and Ni respectively.
1021 The average of the five measurements is 0.0065 emu/(g kOe) for Fe and
1022 0.0025 emu/(g kOe) for Ni. The error is given by the product of χ_{HF} and the
1023 internal field in the foil divided by the saturation magnetization. For Fe (Ni)
1024 foils the field is set to 4 (2) T giving an internal field of 18.4 (13.8) kOe. With
1025 saturation magnetization for Fe (Ni) of 218 (55.2) emu/g this gives a final
1026 percent error of 0.055 (0.063)%. We add this additional error in quadrature
1027 with the error in the orbital fraction propagated from the uncertainty in g' .

Table 5: Measurements of χ_{HF} in the high-field and/or low temperature regime for iron. The measurement by Herring *et al.* is almost 3 times larger than the average of the others. The reason for this is not clear, but this measurement was conservatively retained in the average. The “Error” column is the percent contribution to the magnetization at an applied field of 4 T.

Publication	Material	$\chi_{\text{HF}} \left(\frac{\text{emu}}{\text{g kOe}} \right)$	Error %
Herring <i>et al.</i> 1966 [78]	Fe+4%Si	0.0140	0.118
Foner <i>et al.</i> 1966 [81]	Fe	0.0051	0.043
Stoelinga <i>et al.</i> 1966 [79]	Fe	0.0041	0.035
Foner <i>et al.</i> 1969 [11]	Fe	0.0055	0.046
Pauthenet <i>et al.</i> 1982 [12]	Fe	0.0036	0.031
Average		0.0065	0.055

Table 6: Measurements of χ_{HF} in the high-field and/or low temperature regime for nickel. Once again, the measurement by Herring *et al.* is 3 times larger than the average of the others. The “Error” column is the percent contribution to the magnetization at an applied field of 2 T.

Publication	Material	$\chi_{\text{HF}} \left(\frac{\text{emu}}{\text{g kOe}} \right)$	Error %
Herring <i>et al.</i> 1966 [78]	Ni	0.0056	0.141
Foner <i>et al.</i> 1966 [81]	Ni	0.0012	0.031
Stoelinga <i>et al.</i> 1966 [79]	Ni	0.0023	0.057
Foner <i>et al.</i> 1969 [11]	Ni	0.0019	0.048
Pauthenet <i>et al.</i> 1982 [12]	Ni	0.0016	0.040
Average		0.0025	0.063

3. Calculation of Target Polarization

We are now in a position to calculate the final target polarization and the uncertainty on the value. Tables 7 and 8 provide the data for Fe and Ni respectively. The values for magnetization and polarization are calculated for applied magnetic fields of 4 T and 2 T for Fe and Ni foils respectively. In the calculation of target polarization by deBever *et al.* [3], the magnetic moment of an electron is assumed to be $1 \mu_B$, which is an approximation valid in the limit that $g_S = 2$ since $\mu_e = \frac{g_S}{2} \mu_B$. Thus the magnetic moment of an electron is approximately $1.00116 \mu_B$ and this approximation introduces an error at the 0.1% level.

Temperature corrections due to target heating are calculated for a $1 \mu A$ beam load. To first order, increasing the beam load linearly increases the temperature correction whereas increasing target thickness leaves the temperature unchanged. This insensitivity of temperature to thickness is due to the assumption of a good thermal contact with an infinite heat sink at the foil edge. Under these assumptions, the increased conduction of the thicker foil offsets the additional heat load. Therefore, increasing foil thickness is the better choice for increasing scattering rates.

Table 7: Summary of values and errors involved in calculating the target polarization for Fe foils.

Quantity	T=294 K	T=307 K	Unit
Saturation magnetization M_s	218.04(44)	217.73(45)	emu/g
Saturation magnetization M_s	2.1803(44)	2.1771(45)	μ_B/atom
g'	1.9206(19)	1.9206(19)	—
Orbital fraction: $\frac{M_L}{M_{\text{tot}}} = \frac{g_S - g'}{g'(g_S - 1)}$	0.0425(10)	0.0425(10)	—
Spin component: $M_S \left(1 - \frac{M_L}{M_{\text{tot}}}\right)$	2.0877(47)	2.0847(48)	μ_B/atom
Average electron magnetization	0.08030(18)	0.08018(19)	μ_B
Average electron polarization	0.08020(18)	0.08009(19)	—

Thus we have demonstrated that the saturation polarization of an Fe target can be determined to $\pm 0.23\%$ under a $1 \mu A$ beam load, typical for Hall A at Jefferson Lab. For the same conditions the polarization for a Ni target can be determined to $\pm 0.33\%$. However, it is important to verify

Table 8: Summary of values and errors involved in calculating the target polarization for Ni foils.

Quantity	T=294 K	T=307 K	Unit
Saturation magnetization M_s	55.24(11)	54.91(15)	emu/g
Saturation magnetization M_s	0.5806(12)	0.5771(16)	μ_B/atom
g'	1.8365(30)	1.8365(30)	—
Orbital fraction: $\frac{M_L}{M_{\text{tot}}} = \frac{g_S - g'}{g'(g_S - 1)}$	0.0901(18)	0.0901(18)	—
Spin component: $M_S \left(1 - \frac{M_L}{M_{\text{tot}}}\right)$	0.5283(15)	0.5251(18)	μ_B/atom
Average electron magnetization	0.018867(53)	0.018753(63)	μ_B
Average electron polarization	0.018845(53)	0.018731(63)	—

that the target truly is saturated at the magnetic field settings for a given experiment. Further discussion of this topic including sensitivity to target alignment and flatness are a topic for an additional publication.

A total of $\pm 0.25\%$ is currently allotted in our proposed uncertainty budget for target polarization for the MOLLER experiment, implying that we must demonstrate that we are within 0.1% of saturation for an iron target. Although Ni polarization uncertainty is significantly higher than Fe, a significant contribution that can be greatly reduced comes from the heating correction. The heating correction for Ni is much larger than for Fe due to its low Curie temperature. Reducing the current from 1 to 0.3 μA for a Ni foil reduces the overall systematic error from $\pm 0.33\%$ to $\pm 0.28\%$. Thus, a single precision, low current measurement on a Ni foil could be of value for crosschecking the systematic error on the polarization for Fe.

4. Concluding Discussion

The polarization of a saturated ferromagnetic target has been calculated for both nickel and iron foils. With the stringent demands of the proposed MOLLER experiment, it seemed wise to revisit the study of Fe target polarization by deBever *et al.*[3]. A different approach was taken than that in [3] where instead of using the saturation magnetization value at 0 K and then correcting back to room temperature, measured values of magnetization were taken at or near room temperature. A small error was found in the magnetic field correction in equation (3) of [3] where the applied magnetic field was

used instead of the internal magnetic field, introducing a small error of about 0.1%. Using the approximation $g_S = 2$ also introduced further errors of order 0.1% in [3].

Using measurements of magnetization and g' we calculate the saturation target polarization for Fe foils at room temperature with 4 T fields applied normal to the foil to be 0.08020 ± 0.00018 . For Ni foils under a 2 T applied field, the saturation polarization is 0.018845 ± 0.000053 . We are optimistic that utilizing an Fe foil target will allow us to reach our uncertainty goal of $\pm 0.25\%$ for target polarization including all uncertainties.

Recent evidence from measurement in Hall A revealed our sensitivity to wrinkles in the foil and raised questions about how well our foils were aligned normal to the holding field. Deviations of the foil surface from normality make it more difficult to reach saturation which is the only place where polarization is known with high accuracy. Further studies will be needed and are ongoing to determine the level of foil flatness required and our sensitivity to foil alignment angle. These are topics of discussion for a future publication.

We would like to thank Silviu Covrig of Jefferson Lab for cross-checking our simple target heating model with his ANSYS-Fluent software package. We also acknowledge the support of the U.S. Department of Energy. This material is based upon the work supported by the U.S. Department of Energy, Office of Science, Office of Nuclear Physics Contract No. DE-AC05-06OR23177. Temple University also acknowledges the support of the U.S. Department of Energy, Office of Science, Office of Nuclear Physics under contract DE-SC0020422.

References

- [1] The MOLLER Collaboration, The MOLLER experiment: An ultra-precise measurement of the weak mixing angle using Møller scattering (2014). [arXiv:1411.4088](https://arxiv.org/abs/1411.4088).
- [2] The SoLID collaboration, SoLID (Solenoidal Large Intensity Device) updated preliminary conceptual design report.
URL <https://hallaweb.jlab.org/12GeV/SoLID/files/solid-precdr-Nov2019.pdf>
- [3] L. de Bever, J. Jourdan, M. Loppacher, S. Robinson, I. Sick, J. Zhao, A target for precise Møller polarimetry, Nuclear Instruments and

- 1106 Methods in Physics Research Section A: Accelerators, Spectrometers,
1107 Detectors and Associated Equipment 400 (2) (1997) 379 – 386.
1108 doi:[http://dx.doi.org/10.1016/S0168-9002\(97\)00961-3](http://dx.doi.org/10.1016/S0168-9002(97)00961-3).
1109 URL <http://www.sciencedirect.com/science/article/pii/S0168900297009613>
1110
- 1111 [4] M. Swartz, H. Band, F. Decker, P. Emma, M. Fero, R. Frey,
1112 R. King, A. Lath, T. Limberg, R. Prepost, P. Rowson, B. Schumm,
1113 M. Woods, M. Zolotorev, Observation of target electron momentum
1114 effects in single-arm möller polarimetry, Nuclear Instruments and
1115 Methods in Physics Research Section A: Accelerators, Spectrometers,
1116 Detectors and Associated Equipment 363 (3) (1995) 526–537.
1117 doi:[https://doi.org/10.1016/0168-9002\(95\)00384-3](https://doi.org/10.1016/0168-9002(95)00384-3).
1118 URL <https://www.sciencedirect.com/science/article/pii/0168900295003843>
1119
- 1120 [5] D. Adhikari, *et. al.*, Accurate determination of the neutron skin thick-
1121 ness of ^{208}Pb through parity-violation in electron scattering, Phys. Rev.
1122 Lett. 126 (2021) 172502. doi:[10.1103/PhysRevLett.126.172502](https://doi.org/10.1103/PhysRevLett.126.172502).
1123 URL [https://link.aps.org/doi/10.1103/PhysRevLett.126.](https://link.aps.org/doi/10.1103/PhysRevLett.126.172502)
1124 [172502](https://link.aps.org/doi/10.1103/PhysRevLett.126.172502)
- 1125 [6] Y. Kraftmakher, Spontaneous magnetization of ferromagnets, American
1126 Journal of Physics 73 (12) (2005) 1191–1194. arXiv:<https://doi.org/10.1119/1.1994857>, doi:[10.1119/1.1994857](https://doi.org/10.1119/1.1994857).
1127 URL <https://doi.org/10.1119/1.1994857>
1128
- 1129 [7] C. Kittel, Physical theory of ferromagnetic domains, Rev. Mod. Phys.
1130 21 (1949) 541–583. doi:[10.1103/RevModPhys.21.541](https://doi.org/10.1103/RevModPhys.21.541).
1131 URL <https://link.aps.org/doi/10.1103/RevModPhys.21.541>
- 1132 [8] F. Bloch, Zur theorie des ferromagnetismus, Zeitschrift für Physik 61 (3)
1133 (1930) 206–219. doi:[10.1007/BF01339661](https://doi.org/10.1007/BF01339661).
1134 URL <http://dx.doi.org/10.1007/BF01339661>
- 1135 [9] C. Herring, C. Kittel, On the theory of spin waves in ferromagnetic
1136 media, Phys. Rev. 81 (1951) 869–880. doi:[10.1103/PhysRev.81.869](https://doi.org/10.1103/PhysRev.81.869).
1137 URL <https://link.aps.org/doi/10.1103/PhysRev.81.869>

- 1138 [10] F. J. Dyson, Thermodynamic behavior of an ideal ferromagnet, Phys.
1139 Rev. 102 (1956) 1230–1244. doi:10.1103/PhysRev.102.1230.
1140 URL <https://link.aps.org/doi/10.1103/PhysRev.102.1230>
- 1141 [11] S. Foner, A. J. Freeman, N. A. Blum, R. B. Frankel, E. J. McNiff, H. C.
1142 Praddaude, High-field studies of band ferromagnetism in Fe and Ni by
1143 Mössbauer and magnetic moment measurements, Phys. Rev. 181 (1969)
1144 863–882. doi:10.1103/PhysRev.181.863.
1145 URL <https://link.aps.org/doi/10.1103/PhysRev.181.863>
- 1146 [12] R. Pauthenet, Spin-waves in nickel, iron, and yttrium-iron garnet, Jour-
1147 nal of Applied Physics 53 (3) (1982) 2029–2031. doi:10.1063/1.
1148 330694.
1149 URL <http://dx.doi.org/10.1063/1.330694>
- 1150 [13] F. J. Dyson, General theory of spin-wave interactions, Phys. Rev. 102
1151 (1956) 1217–1230. doi:10.1103/PhysRev.102.1217.
1152 URL <https://link.aps.org/doi/10.1103/PhysRev.102.1217>
- 1153 [14] F. Keffer, Spin Waves, Springer, Berlin, Heidelberg, 1966, pp. 1–273.
1154 doi:https://doi.org/10.1007/978-3-642-46035-7_1.
- 1155 [15] R. Pauthenet, Experimental verification of spin-wave theory in high
1156 fields (invited), Journal of Applied Physics 53 (11) (1982) 8187–8192.
1157 doi:10.1063/1.330287.
1158 URL <http://dx.doi.org/10.1063/1.330287>
- 1159 [16] C. D. G. Jr., Iron and nickel as magnetization standards, Journal of
1160 Applied Physics 53 (3) (1982) 2032–2034. doi:10.1063/1.330695.
1161 URL <http://dx.doi.org/10.1063/1.330695>
- 1162 [17] R. Skomski, G. C. Hadjipanayis, D. J. Sellmyer, Effective demagnetizing
1163 factors of complicated particle mixtures, IEEE Transactions on Magnet-
1164 ics 43 (6) (2007) 2956–2958. doi:10.1109/TMAG.2007.893798.
- 1165 [18] E. A. Owen, D. M. Jones, Effect of grain size on the crystal structure
1166 of cobalt, Proceedings of the Physical Society. Section B 67 (6) (1954)
1167 456.
1168 URL <http://stacks.iop.org/0370-1301/67/i=6/a=302>

- 1169 [19] W. E. Case, R. D. Harrington, Calibration of vibrating-sample magne-
 1170 tometers, Journal of Research of the National Bureau of Standards-C
 1171 Engineering and Instrumentation 70C (4) (1966) 255–262.
 1172 URL [http://nvlpubs.nist.gov/nistpubs/jres/70C/
 1173 jresv70Cn4p255_A1b.pdf](http://nvlpubs.nist.gov/nistpubs/jres/70C/jresv70Cn4p255_A1b.pdf)
- 1174 [20] J. Crangle, G. M. Goodman, The magnetization of pure iron and
 1175 nickel, Proceedings of the Royal Society of London A: Mathemati-
 1176 cal, Physical and Engineering Sciences 321 (1547) (1971) 477–491.
 1177 doi:10.1098/rspa.1971.0044.
 1178 URL [http://rspa.royalsocietypublishing.org/content/321/
 1179 1547/477](http://rspa.royalsocietypublishing.org/content/321/1547/477)
- 1180 [21] H. Danan, A. Herr, A. J. P. Meyer, New determinations of the saturation
 1181 magnetization of nickel and iron, Journal of Applied Physics 39 (2)
 1182 (1968) 669–670. doi:10.1063/1.2163571.
 1183 URL <http://dx.doi.org/10.1063/1.2163571>
- 1184 [22] A. T. Aldred, Temperature dependence of the magnetization of nickel,
 1185 Phys. Rev. B 11 (1975) 2597–2601. doi:10.1103/PhysRevB.11.2597.
 1186 URL <https://link.aps.org/doi/10.1103/PhysRevB.11.2597>
- 1187 [23] P. Weiss, R. Forrer, La saturation absolue des ferromagnétiques et les
 1188 lois d’approche en fonction du champ et de la température, Ann. Phys.
 1189 10 (12) (1929) 279–372. doi:10.1051/anphys/192910120279.
 1190 URL <https://doi.org/10.1051/anphys/192910120279>
- 1191 [24] R. L. Sanford, E. G. Bennett, A determination of the magnetic satura-
 1192 tion induction of iron at room temperature, NIST Journal of Research
 1193 (Jan 1941).
 1194 URL [http://nistdigitalarchives.contentdm.oclc.org/cdm/ref/
 1195 collection/p13011coll16/id/104774](http://nistdigitalarchives.contentdm.oclc.org/cdm/ref/collection/p13011coll16/id/104774)
- 1196 [25] H. Danan, On the interpretation of the magnetization measurements
 1197 of pure polycrystalline iron and nickel in the vicinity of saturation,
 1198 J. Phys. Radium 20 (2-3) (1959) 203–207. doi:10.1051/jphysrad:
 1199 01959002002-3020300.
 1200 URL <https://hal.archives-ouvertes.fr/jpa-00236018>

- 1201 [26] S. Arajs, G. R. Dunmyre, A note on the consistency of values of the
 1202 spontaneous or saturation magnetization of polycrystalline iron and
 1203 nickel at 298 °K, *Physica Status Solidi (b)* 21 (1) (1967) 191–195.
 1204 doi:10.1002/pssb.19670210117.
 1205 URL <http://dx.doi.org/10.1002/pssb.19670210117>
- 1206 [27] D. R. Behrendt, D. E. Hegland, Saturation magnetization of polycrys-
 1207 talline iron, Tech. rep., NASA (Apr 1972).
 1208 URL <https://ntrs.nasa.gov/search.jsp?R=19720015089>
- 1209 [28] C. S. Edmund, Ferromagnetism: magnetization curves, *Reports on*
 1210 *Progress in Physics* 13 (1) (1950) 83–183. doi:10.1088/0034-4885/
 1211 13/1/304.
 1212 URL <https://doi.org/10.1088/0034-4885/13/1/304>
- 1213 [29] S. Foner, Hall effect and magnetic properties of armco iron, *Phys. Rev.*
 1214 101 (1956) 1648–1652. doi:10.1103/PhysRev.101.1648.
 1215 URL <https://link.aps.org/doi/10.1103/PhysRev.101.1648>
- 1216 [30] B. D. Cullity, C. D. Graham, *Introduction to Magnetic Materials*, 2nd
 1217 Edition, Wiley-IEEE Press, 2008.
- 1218 [31] H. P. Myers, W. Sucksmith, The spontaneous magnetization of
 1219 cobalt, *Proceedings of the Royal Society of London A: Mathemat-*
 1220 *ical, Physical and Engineering Sciences* 207 (1091) (1951) 427–446.
 1221 arXiv:[http://rspa.royalsocietypublishing.org/content/207/](http://rspa.royalsocietypublishing.org/content/207/1091/427.full.pdf)
 1222 [1091/427.full.pdf](http://rspa.royalsocietypublishing.org/content/207/1091/427.full.pdf), doi:10.1098/rspa.1951.0132.
 1223 URL [http://rspa.royalsocietypublishing.org/content/207/](http://rspa.royalsocietypublishing.org/content/207/1091/427)
 1224 [1091/427](http://rspa.royalsocietypublishing.org/content/207/1091/427)
- 1225 [32] J. D. C., Solutions to the heat equation for circular target foil heating
 1226 by an electron beam for uniform and gaussian beam distributions.
 1227 URL [https://moller.jlab.org/DocDB/0008/000874/001/](https://moller.jlab.org/DocDB/0008/000874/001/TargetHeating.pdf)
 1228 [TargetHeating.pdf](https://moller.jlab.org/DocDB/0008/000874/001/TargetHeating.pdf)
- 1229 [33] S. Arajs, R. V. Colvin, Ferromagnetic-paramagnetic transition in iron,
 1230 *Journal of Applied Physics* 35 (8) (1964) 2424–2426. doi:10.1063/1.
 1231 1702873.
 1232 URL <http://dx.doi.org/10.1063/1.1702873>

- 1233 [34] S. Arajs, R. Colvin, Paramagnetism of polycrystalline nickel, Journal
1234 of Physics and Chemistry of Solids 24 (10) (1963) 1233 – 1237.
1235 doi:[http://dx.doi.org/10.1016/0022-3697\(63\)90242-7](http://dx.doi.org/10.1016/0022-3697(63)90242-7).
1236 URL [http://www.sciencedirect.com/science/article/pii/](http://www.sciencedirect.com/science/article/pii/0022369763902427)
1237 0022369763902427
- 1238 [35] S. Arajs, Paramagnetic behavior of nickel just above the ferromagnetic
1239 curie temperature, Journal of Applied Physics 36 (3) (1965) 1136–1137.
1240 doi:10.1063/1.1714136.
1241 URL <http://dx.doi.org/10.1063/1.1714136>
- 1242 [36] F. E. Luborsky, J. L. Walter, E. P. Wohlfarth, The saturation mag-
1243 netisation, curie temperature and size effect of amorphous iron alloys,
1244 Journal of Physics F: Metal Physics 10 (5) (1980) 959.
1245 URL <http://stacks.iop.org/0305-4608/10/i=5/a=024>
- 1246 [37] S. A. Ahern, M. J. C. Martin, W. Sucksmith, The spontaneous mag-
1247 netization of nickel+copper alloys, Proceedings of the Royal Society of
1248 London. Series A, Mathematical and Physical Sciences 248 (1253) (1958)
1249 145–152.
1250 URL <http://www.jstor.org/stable/100593>
- 1251 [38] P. R. Locher, S. Geschwind, Electron-nuclear double resonance of Fe⁵⁷
1252 in MgO, Phys. Rev. 139 (1965) A991–A994. doi:10.1103/PhysRev.
1253 139.A991.
1254 URL <https://link.aps.org/doi/10.1103/PhysRev.139.A991>
- 1255 [39] M. Norgett, M. Robinson, I. Torrens, A proposed method of calculating
1256 displacement dose rates, Nuclear Engineering and Design 33 (1) (1975)
1257 50–54. doi:[https://doi.org/10.1016/0029-5493\(75\)90035-7](https://doi.org/10.1016/0029-5493(75)90035-7).
1258 URL [https://www.sciencedirect.com/science/article/pii/](https://www.sciencedirect.com/science/article/pii/0029549375900357)
1259 0029549375900357
- 1260 [40] O. W. Richardson, A mechanical effect accompanying magnetiza-
1261 tion, Phys. Rev. (Series I) 26 (1908) 248–253. doi:10.1103/
1262 PhysRevSeriesI.26.248.
1263 URL <https://link.aps.org/doi/10.1103/PhysRevSeriesI.26.248>
- 1264 [41] G. G. Scott, Review of Gyromagnetic Ratio Experiments, Reviews of
1265 Modern Physics 34 (1962) 102–109. doi:10.1103/RevModPhys.34.102.

- 1266 [42] S. J. Barnett, On magnetization by angular acceleration (Sep. 1909).
 1267 doi:10.1126/science.30.769.413.
 1268 URL <https://doi.org/10.1126/science.30.769.413>
- 1269 [43] S. J. Barnett, New researches on magnetization by rotation and the gy-
 1270 romagnetic ratios of ferromagnetic substances, Proceedings of the Amer-
 1271 ican Academy of Arts and Sciences 75 (5) (1944) 109–129.
 1272 URL <http://www.jstor.org/stable/20023462>
- 1273 [44] C. Kittel, On the gyromagnetic ratio and spectroscopic splitting factor
 1274 of ferromagnetic substances, Phys. Rev. 76 (1949) 743–748. doi:10.
 1275 1103/PhysRev.76.743.
 1276 URL <https://link.aps.org/doi/10.1103/PhysRev.76.743>
- 1277 [45] A. J. P. Meyer, G. Asch, Experimental g' and g values of Fe, Co, Ni,
 1278 and their alloys, Journal of Applied Physics 32 (3) (1961) S330–S333.
 1279 doi:10.1063/1.2000457.
 1280 URL <http://dx.doi.org/10.1063/1.2000457>
- 1281 [46] J. Smit, H. Wijn, Ferrites, Eindhoven: Philips Technical Library, 1959.
- 1282 [47] M. Phillips, The effect of nuclear motion on atomic magnetic moments,
 1283 Phys. Rev. 76 (1949) 1803–1804. doi:10.1103/PhysRev.76.1803.
 1284 URL <https://link.aps.org/doi/10.1103/PhysRev.76.1803>
- 1285 [48] G. G. Scott, A precise mechanical measurement of the gyromagnetic
 1286 ratio of iron, Phys. Rev. 82 (1951) 542–547. doi:10.1103/PhysRev.
 1287 82.542.
 1288 URL <https://link.aps.org/doi/10.1103/PhysRev.82.542>
- 1289 [49] S. J. Barnett, G. S. Kenny, Gyromagnetic ratios of iron, cobalt, and
 1290 many binary alloys of iron, cobalt, and nickel, Phys. Rev. 87 (1952)
 1291 723–734. doi:10.1103/PhysRev.87.723.
 1292 URL <https://link.aps.org/doi/10.1103/PhysRev.87.723>
- 1293 [50] Meyer, André J.P., Brown, Sheldon, Nouvelles mesures des rapports
 1294 gyromagnétiques du fer et du nickel, J. Phys. Radium 18 (3) (1957)
 1295 161–168. doi:10.1051/jphysrad:01957001803016100.
 1296 URL <https://doi.org/10.1051/jphysrad:01957001803016100>

- 1297 [51] G. G. Scott, Gyromagnetic ratios of Fe and Ni, Phys. Rev. 119 (1960)
1298 84–85. doi:10.1103/PhysRev.119.84.
1299 URL <https://link.aps.org/doi/10.1103/PhysRev.119.84>
- 1300 [52] E. Wohlfarth, Chapter 1 iron, cobalt and nickel, Handbook of Ferro-
1301 magnetic Materials 1 (1980) 35. doi:http://dx.doi.org/10.1016/
1302 S1574-9304(05)80116-6.
1303 URL [http://www.sciencedirect.com/science/article/pii/
1304 S1574930405801166](http://www.sciencedirect.com/science/article/pii/S1574930405801166)
- 1305 [53] D. Bonnenberg, K. A. Hempel, H. Wijn, 1.2.1.2.4 Atomic magnetic mo-
1306 ment, magnetic moment density, g and g' factor, Springer Berlin Heidel-
1307 berg, Berlin, Heidelberg, 1986, pp. 174–188. doi:10.1007/10311893_
1308 25.
1309 URL https://doi.org/10.1007/10311893_25
- 1310 [54] G. G. Scott, H. W. Sturmer, Magnetomechanical ratios for Fe-Co alloys,
1311 Phys. Rev. 184 (1969) 490–491. doi:10.1103/PhysRev.184.490.
1312 URL <https://link.aps.org/doi/10.1103/PhysRev.184.490>
- 1313 [55] L. Püst, Z. Frait, Low-temperature FMR and FMAR measurements of
1314 tetal single crystals. I. General Consideration, Experimental Techniques,
1315 Physica Status Solidi (b) 122 (2) (1984) 535–541. doi:10.1002/pssb.
1316 2221220218.
1317 URL <http://dx.doi.org/10.1002/pssb.2221220218>
- 1318 [56] M. *et al.* Tanabashi, Review of particle physics, Phys. Rev. D 98 (2018)
1319 030001. doi:10.1103/PhysRevD.98.030001.
1320 URL <https://link.aps.org/doi/10.1103/PhysRevD.98.030001>
- 1321 [57] J. H. Van Vleck, Concerning the theory of ferromagnetic resonance ab-
1322 sorption, Phys. Rev. 78 (1950) 266–274. doi:10.1103/PhysRev.78.266.
1323 URL <https://link.aps.org/doi/10.1103/PhysRev.78.266>
- 1324 [58] R. A. Reck, D. L. Fry, Orbital and spin magnetization in Fe-Co, Fe-
1325 Ni, and Ni-Co, Phys. Rev. 184 (1969) 492–495. doi:10.1103/PhysRev.
1326 184.492.
1327 URL <https://link.aps.org/doi/10.1103/PhysRev.184.492>

- 1328 [59] G. G. Scott, Gyromagnetic ratio of nickel at low magnetic intensities,
1329 Phys. Rev. 99 (1955) 1824–1825. doi:10.1103/PhysRev.99.1824.
1330 URL <https://link.aps.org/doi/10.1103/PhysRev.99.1824>
- 1331 [60] K. J. Standley, K. H. Reich, Ferromagnetic resonance in nickel and in
1332 some of its alloys, Proceedings of the Physical Society. Section B 68 (10)
1333 (1955) 713.
1334 URL <http://stacks.iop.org/0370-1301/68/i=10/a=303>
- 1335 [61] A. Borovik-Romanov, S. Sinha, Spin Waves and Magnetic Excitations,
1336 no. 2 in Modern problems in condensed matter sciences, North-Holland,
1337 1988.
1338 URL <https://books.google.com/books?id=Qj9BAQAAIAAJ>
- 1339 [62] C. J. Gadsden, M. Heath, Ferromagnetic resonance of nickel vanadium
1340 alloys, Journal of Physics F: Metal Physics 8 (3) (1978) 521.
1341 URL <http://stacks.iop.org/0305-4608/8/i=3/a=021>
- 1342 [63] B. D. Shanina, V. G. Gavriljuk, A. A. Konchits, S. P. Kolesnik, The
1343 influence of substitutional atoms upon the electron structure of the iron-
1344 based transition metal alloys, Journal of Physics: Condensed Matter
1345 10 (8) (1998) 1825.
1346 URL <http://stacks.iop.org/0953-8984/10/i=8/a=015>
- 1347 [64] G. Dewar, B. Heinrich, J. F. Cochran, Ferromagnetic antiresonance
1348 transmission of 24 GHz radiation through nickel (20 to 364 °c), Cana-
1349 dian Journal of Physics 55 (9) (1977) 821–833. doi:10.1139/p77-112.
1350 URL <https://doi.org/10.1139/p77-112>
- 1351 [65] L. Püst, Z. Frait, Precise g-factor determination of Fe-3wt%Si single
1352 crystals in the temperature range 3.5 - 300 K by electron FMR
1353 and FMAR measurements, Physics Letters A 86 (1) (1981) 48 – 50.
1354 doi:[http://dx.doi.org/10.1016/0375-9601\(81\)90685-X](http://dx.doi.org/10.1016/0375-9601(81)90685-X).
1355 URL <http://www.sciencedirect.com/science/article/pii/037596018190685X>
1356
- 1357 [66] S. Haraldson, L. Pettersson, Ferromagnetic resonance in nickel around
1358 the curie temperature, Journal of Physics and Chemistry of Solids 42 (8)
1359 (1981) 681 – 686. doi:[http://dx.doi.org/10.1016/0022-3697\(81\)](http://dx.doi.org/10.1016/0022-3697(81)90121-9)
1360 [90121-9](http://dx.doi.org/10.1016/0022-3697(81)90121-9).

- 1361 URL [http://www.sciencedirect.com/science/article/pii/](http://www.sciencedirect.com/science/article/pii/0022369781901219)
1362 0022369781901219
- 1363 [67] D. Bastian, E. Biller, Anisotropy constants and g-factors of NiFe alloys
1364 derived from ferromagnetic resonance, *physica status solidi (a)* 35 (2)
1365 (1976) 465–470. doi:10.1002/pssa.2210350207.
1366 URL <http://dx.doi.org/10.1002/pssa.2210350207>
- 1367 [68] D. S. Rodbell, Ferromagnetic resonance absorption linewidth of nickel
1368 metal. Evidence for Landau-Lifshitz damping, *Phys. Rev. Lett.* 13 (1964)
1369 471–474. doi:10.1103/PhysRevLett.13.471.
1370 URL <https://link.aps.org/doi/10.1103/PhysRevLett.13.471>
- 1371 [69] D. S. Rodbell, Ferromagnetic resonance of iron whisker crystals, *Journal*
1372 *of Applied Physics* 30 (4) (1959) S187–S188. doi:10.1063/1.2185880.
1373 URL <http://dx.doi.org/10.1063/1.2185880>
- 1374 [70] D. M. S. Bagguley, N. J. Harrick, The temperature dependence of fer-
1375 romagnetic resonance in colloidal nickel, *Proceedings of the Physical*
1376 *Society. Section A* 67 (7) (1954) 648.
1377 URL <http://stacks.iop.org/0370-1298/67/i=7/a=115>
- 1378 [71] N. Bloembergen, On the ferromagnetic resonance in nickel and su-
1379 permalloy, *Phys. Rev.* 78 (1950) 572–580. doi:10.1103/PhysRev.78.
1380 572.
1381 URL <https://link.aps.org/doi/10.1103/PhysRev.78.572>
- 1382 [72] G. G. Scott, Gyromagnetic ratio of iron at low magnetic intensities,
1383 *Phys. Rev.* 99 (1955) 1241–1244. doi:10.1103/PhysRev.99.1241.
1384 URL <https://link.aps.org/doi/10.1103/PhysRev.99.1241>
- 1385 [73] G. G. Scott, Gyromagnetic ratios of the iron-nickel alloys, *Phys. Rev.*
1386 103 (1956) 561–563. doi:10.1103/PhysRev.103.561.
1387 URL <https://link.aps.org/doi/10.1103/PhysRev.103.561>
- 1388 [74] FRAIT, Z., GEMPERLE, R., The g-factor and surface magnetization of
1389 pure iron along [100] and [111] directions, *J. Phys. Colloques* 32 (1971).
1390 doi:10.1051/jphyscol:19711182.
1391 URL <https://doi.org/10.1051/jphyscol:19711182>

- 1392 [75] C. Kittel, On the theory of ferromagnetic resonance absorption, Phys.
1393 Rev. 73 (1948) 155–161. doi:10.1103/PhysRev.73.155.
1394 URL <https://link.aps.org/doi/10.1103/PhysRev.73.155>
- 1395 [76] Z. Frait, The g-factor in pure polycrystalline iron, Czechoslovak Journal
1396 of Physics B 27 (2) (1977) 185–189. doi:10.1007/BF01587010.
1397 URL <https://doi.org/10.1007/BF01587010>
- 1398 [77] Z. Frait, H. MacFaden, Ferromagnetic resonance in metals. Frequency
1399 dependence, Phys. Rev. 139 (1965) A1173–A1181. doi:10.1103/
1400 PhysRev.139.A1173.
1401 URL <https://link.aps.org/doi/10.1103/PhysRev.139.A1173>
- 1402 [78] C. Herring, R. M. Bozorth, A. E. Clark, T. R. McGuire, High-field sus-
1403 ceptibilities of iron and nickel, Journal of Applied Physics 37 (3) (1966)
1404 1340–1341. arXiv:<https://doi.org/10.1063/1.1708462>, doi:10.
1405 1063/1.1708462.
1406 URL <https://doi.org/10.1063/1.1708462>
- 1407 [79] J. Stoelinga, R. Gersdorf, Field dependence of the magnetization in high
1408 fields for bcc fe-co and fe-ni alloys, Physics Letters 19 (8) (1966) 640–641.
- 1409 [80] M. Yasui, M. Shimizu, Calculations of orbital paramagnetic susceptibil-
1410 ity for vanadium, chromium and iron, Journal of the Physical Society
1411 of Japan 31 (2) (1971) 378–381. arXiv:<https://doi.org/10.1143/JPSJ.31.378>,
1412 JPSJ.31.378, doi:10.1143/JPSJ.31.378.
1413 URL <https://doi.org/10.1143/JPSJ.31.378>
- 1414 [81] A. J. Freeman, N. A. Blum, S. Foner, R. B. Frankel, E. J. Mc-
1415 Niff, Ferromagnetic metals in high magnetic fields, Journal of Applied
1416 Physics 37 (3) (1966) 1338–1339. arXiv:[https://doi.org/10.1063/](https://doi.org/10.1063/1.1708461)
1417 1.1708461, doi:10.1063/1.1708461.
1418 URL <https://doi.org/10.1063/1.1708461>